Coronaviruses using different strategies to antagonize antiviral responses and pyroptosis

Xinyu Fu[1,7], Yang Yang[2,7], Weilv Xu[1,3,4,7], Danyue Li[1,3,4,7], Xinyue Li[1,3,4], Nan Chen[1,3,4], Qian Lv[1,3,4], Yuhua Shi[1,3,4], Xiaoliang Li [1,4,5,*] Fushan Shi,[1,3,4,6,*]

[1] Department of Veterinary Medicine, College of Animal Sciences, Zhejiang University, Hangzhou 310058, Zhejiang, China

[2] Key Laboratory of Applied Technology on Green-Eco-Healthy Animal Husbandry of Zhejiang Province, Zhejiang Provincial Engineering Research Center for Animal Health Diagnostics & Advanced Technology, Zhejiang International Science and Technology Cooperation Base for Veterinary Medicine and Health Management, China-Australia Joint Laboratory for Animal Health Big Data Analytics, College of Animal Science and Technology & College of Veterinary Medicine of Zhejiang A&F University, Hangzhou 310058, Zhejiang, China

[3] MOA Key Laboratory of Animal Virology, Center for Veterinary Sciences, Zhejiang University, Hangzhou 310058, Zhejiang, China

[4] Institute of Preventive Veterinary Medicine, Zhejiang Provincial Key Laboratory of Preventive Veterinary Medicine, Zhejiang University, Hangzhou 310058, Zhejiang, China

[5] Hainan Institute of Zhejiang University, Sanya 572025, Hainan, China

[6] Veterinary Teaching Hospital, Center for Veterinary Sciences, Zhejiang University, Hangzhou 310058, Zhejiang, China

[7] These authors contributed equally to this work

[*] Corresponding author: Xiaoliang Li, E-mail: xlli@zju.edu.cn; Fushan Shi, E-mail: sfs@zju.edu.cn

Abstract

Viral infection triggers inflammasome-mediated caspase-1 activation. However, less is known about how viruses use the active caspase-1 to evade host immune response. Here, we use porcine epidemic diarrhea virus (PEDV) as a model of coronaviruses (CoVs) to illustrate the sophisticated regulation of CoVs to counteract IFN-I signaling and pyroptosis. We show that PEDV infection stabilizes caspase-1 expression via papain-like protease PLP2's deubiquitinase activity and the enhanced stabilization of caspase-1 disrupts IFN-I signaling by cleaving RIG-I at D189 residue. Meanwhile, PLP2 can degrade GSDMD-p30 by removing its K27-linked ubiquitin chain at K275 to restrain pyroptosis. Papain-like proteases from other genera of CoVs (PDCoV and SARS-CoV-2) have the similar activity to degrade GSDMD-p30. We further demonstrate that SARS-CoV-2 N protein induced NLRP3 inflammasome activation also uses the active caspase-1 to counter IFN-I signaling by cleaving RIG-I. Therefore, our work unravels a novel antagonistic mechanism employed by CoVs to evade host antiviral response.

Keywords: Coronavirus; Papain-like protease; Antiviral immunity; GSDMD; Type I interferon signaling

Introduction

Coronaviruses which belong to order Nidovirales, family Coronaviridae, and subfamily Orthocoronavirinae, are a group of viruses packaged in envelop covered with spikes and contain a linear, single and positive-stranded RNA[1]. Coronaviruses

are subdivided into four genera, including α, β, γ, and δ. As a member of α genus, PEDV infection was characterized by vomiting, severe diarrhea, dehydration and high mortality in suckling piglets[2]. The viral genome of PEDV contains a full-length genome of 28 kb and encodes a total of seven open reading frames (ORFs)[3]. Like other CoVs, PEDV utilizes its own proteases, including papain-like protease (PLpro) and main protease to cleave the polyprotein. The papain-like protease of PEDV is encoded by the largest nonstructural protein Nsp3, which contains two papain-like protease domains (PLP1 and PLP2 or PLpro)[4]. In general, α coronaviruses and clade A of β coronaviruses harbor PLP1 and PLP2, and other coronaviruses have one functional PLpro only[5]. Studies have shown that CoVs PLP2 (PLpro) act as a viral deubiquitinase to negatively regulate type I IFN signaling pathway[4,6]. For example, mouse hepatitis virus (MHV) PLP2 can bind to and deubiquitinate IRF3 to prevent its nuclear translocation[7]. Transmissible gastroenteritis virus (TGEV) PLP2 is able to inhibit the degradation of IκBα by decreasing its ubiquitination, resulting in the suppression of NF-κB signaling[8]. As to PEDV PLP2, it has been reported that PLP2 deubiquitinates RIG-I and STING to block the IFN signaling pathway[4]. The catalytically dead mutants of PLP2 (C1729A, H1888A and D1901A) can abrogate their deubiquitinase activity and fail to inhibit PEDV-induced IFN-β production.

Caspase-1 is a cysteine protein hydrolase, which participates in cell death and inflammatory response[9]. Caspase-1 exists in the form of proteasome (pro-caspase-1) at static state and acts as an enzyme after activation, which relies on the activation of different inflammasomes[10]. Interestingly, high expression of pro-caspase-1 can also

result in its auto-activation in the absence of a ligand[11-13]. Pyroptosis is an inflammatory caspases-dependent, pro-inflammatory programmed cell death characterized by losing of cell membrane integrity, pore forming and swelling and rupture of the cells[14]. The canonical pathway of pyroptosis is mediated by caspase-1[15,16]. When host cells' pattern-recognition receptors (PRRs) are stimulated by pathogen-associated molecular patterns (PAMPs) or damage-associated molecular patterns (DAMPs), inflammasomes will assemble automatically and activate themselves, leading to the activation of caspase-1. Researches have demonstrated that NLRP3 inflammasome can be activated by ZIKA[17], SARS-CoV-2[18] and MERS-CoV[19,20], and AIM2 inflammasome can be activated by SARS-CoV-2[21] while NLRP1 inflammasome can be activated by human rhinovirus (HRV) and picornaviruses[22]. Activated caspase-1 cleaves GSDMD to produce N-terminal GSDMD-p30 fragments with perforating activity on cell membrane, which leads to pyroptosis, and it also cleaves pro-IL-1β to produce IL-1β to improve antiviral capacity[15,16].

What is clear is that, inflammasomes-mediated caspase-1 activation and pyroptosis induced by viruses will lead to enhancement of cell antiviral capability and destruction of cell integrity, and these changes are detrimental to virus replication, especially at the early stage of viral infection. So what is the purpose of viral activation of caspase-1 as well as pyroptosis? Here, we report that PEDV infection increases the stabilization of caspase-1 by removing its K11-linked ubiquitin chains at K134 via its papain-like protease PLP2. Consequently, caspase-1 targets to RIG-I for

91 cleavage at D189 residue which leads to decreased IFN-I signaling and enhanced
92 PEDV replication. Meanwhile, to assure the integrity of host cells which might be
93 broken by GSDMD-p30 cleaved by caspase-1, PLP2 can degrade GSDMD-p30 by
94 removing its K27-linked ubiquitin chain at K275 residue to restrain pyroptosis. We
95 further demonstrate that papain-like proteases from other genera of CoVs, such as
96 PDCoV and SARS-CoV-2, have the similar activity to degrade GSDMD-p30.
97 Importantly, we confirm that SARS-CoV-2 N protein induced NLRP3 inflammasome
98 activation also uses the active caspase-1 to counter IFN-I signaling. Therefore, our
99 findings uncover a distinctive feature of papain-like protease in antagonizing antiviral
100 responses that might serve as a target for CoVs treatment in the future.
101

102 ## Results

103 **PEDV infection elevates the expression of caspase-1**

104 In order to investigate the effect of PEDV on porcine caspase-1, endogenous
105 caspase-1 expression was analyzed by immunoblotting in intestinal tissues of
106 mock-infected and PEDV naturally-infected piglets. The results showed that
107 expression of caspase-1 was increased in the PEDV-infected piglets (Fig. 1A).
108 qRT-PCR showed that *caspase-1* mRNA abundance was not altered in IPEC-J2 cells
109 upon PEDV infection (Fig. 1B). Immunoblotting also confirmed that PEDV infection
110 promoted the amount of caspase-1 in IPEC-J2 cells and CHX treatment further
111 elevated caspase-1 expression (Fig. 1C), suggesting that the increased caspase-1
112 expression was not caused by the transcription of mRNA and synthesis of new

113 proteins. In addition, Vero cells were transfected with plasmids encoding caspase-1
114 and then infected with PEDV. We found that the increased caspase-1 by PEDV
115 infection was both MOI and time dependent (Fig. 1D and E). Since the high
116 expression of caspsae-1 causes auto-activation and produces active caspase-1 p20[11-13],
117 which can lead to the cleavage of GSDMD, we investigated the relationship between
118 PEDV infection and pyroptosis. Vero cells were co-transfected with GSDMD-FL (full
119 length) and caspase-1 and then infected with PEDV. Caspase-1 expression and
120 cleavage of GSDMD increased progressively in both MOI and time dependent
121 manner during infection (Fig. 1F and G). Interestingly, PEDV infection resulted in
122 declines in LDH release compared to mock-infected group, despite the increased
123 GSDMD cleavage (Fig. 1H and I). These results indicate that PEDV infection
124 promotes the amount of caspase-1.
125

126 **The papain-like protease 2 of PEDV inhibits the proteasomal degradation of**
127 **caspase-1**

128 The increased expression of caspase-1 induces GSDMD cleavage but inhibits
129 pyroptosis. Therefore, we speculated that some kind of viral proteins affected this
130 process. Vero cells transfected with GSDMD-FL were infected with PEDV, following
131 performed with coimmunoprecipitation (Co-IP) and mass spectrometry (MS) analysis.
132 The database search revealed that the papain-like protease 2 (PLP2) of PEDV binds to
133 GSDMD-FL during infection (Supplementary Fig. 1A). The Co-IP assay also
134 confirmed that PEDV PLP2 interacted with GSDMD-FL (Supplementary Fig. 1B).

135 Since it is known that GSDMD-FL and caspase-1 are interacted[23], we further
136 examined whether PLP2 interacts with caspase-1. HEK293T cells were co-transfected
137 with FLAG-tagged caspase-1 and MYC-tagged PLP2, following treated with VX765,
138 an inhibitor of caspase-1, to curb caspase-1 activation. Co-IP assay showed that PLP2
139 interacted with caspase-1 (Supplementary Fig. 1C). Indirect immunofluorescence
140 further demonstrated that GSDMD, caspase-1 and PEDV PLP2 were colocalized in
141 the cytoplasm (Supplementary Fig. 1D). Thus, PLP2 interacts with both caspase-1 and
142 GSDMD.

143 Given that high expression of caspase-1 leads to auto-activation, caspase-1-C285A
144 (caspase-1 mutant, which lacks its protease activity) and PLP2 were co-transfected
145 into HEK293T cells. As shown in Fig. 2A, we observed an increased protein amount
146 of caspase-1-C285A in the presence of PLP2. In addition, co-transfection of PLP2,
147 GSDMD-FL and caspase-1 in HEK293T also revealed that PLP2 caused the
148 accumulation of caspase-1 but not GSDMD-FL (Supplementary Fig. 2A). We next
149 measured caspase-1 degradation by a cycloheximide (CHX) chase assay to determine
150 whether PLP2 could stabilize caspase-1. The results demonstrated that PEDV PLP2
151 could stabilize caspase-1 but not GSDMD-FL by delaying its degradation (Fig. 2B
152 and Supplementary Fig. 2B). Ubiquitination is a key signal for proteasomal
153 degradation, and PLP2 has the deubiquitinase activity. To identify whether the
154 deubiquitinase activity of PLP2 is required for the stabilization of caspase-1, we
155 generated the catalytic mutants (C113A, H272A, D285A) of PLP2 and co-transfected
156 them with caspase-1-C285A. As expected, all of the three mutants lost the ability to

157 stabilize caspase-1 (Fig. 2C). Furthermore, we co-expressed the wild type PLP2 or its
158 mutants with HA-tagged ubiquitin (HA-Ub) and FLAG-tagged caspase-1 in
159 HEK293T cells. Compared to the empty vector, wild type PLP2 substantially
160 inhibited ubiquitination of caspase-1 while the three mutants had no effect on it (Fig.
161 2D), suggesting that the deubiquitinase activity of PLP2 is indispensable for the
162 stabilization of caspase-1.

163 It has been reported that the K11-linked ubiquitination of human caspase-1 at
164 Lys-134 is a way to induce its degradation[24]. To determine whether K134 residue of
165 porcine-derived caspase-1 is also critical for its ubiquitination, we constructed
166 porcine-derived caspase-1-K134R mutant in which the lysine (K) residue was
167 replaced with arginine (R). As shown in Fig. 2E, wild type caspase-1 was degraded by
168 K11 in a dose-dependent manner, while caspase-1-K134R could not be degraded by
169 K11. Moreover, we found that caspase-1-K134R mutant exhibited a dramatic decrease
170 in K11-linked ubiquitination (Supplementary Fig. 2C). To further confirm the role of
171 PLP2 in this process, we co-expressed PLP2 with caspase-1 and K11 ubiquitin, the
172 results demonstrated that the degradation effect of K11 on caspase-1 was abrogated by
173 PLP2 (Fig. 2F). Immunoblotting also showed that PLP2 stabilized caspase-1 but not
174 caspase-1-K134R (Fig. 2G). Additionally, PEDV infection decreased K11-linked
175 poly-ubiquitination of caspase-1, further fortifying the above findings (Fig. 2H).
176 Taken together, these results indicate that PLP2 of PEDV stabilizes porcine caspase-1
177 by removing K11-linked ubiquitin chains at Lys134.

178

179 **Caspase-1 attenuates IFN-I signaling during PEDV infection**

180 It has been reported that caspase-1 can negatively regulate IFN-I signaling by
181 cleaving cGAS during DNA virus infection[25]. As an RNA virus, PEDV activates
182 IFN-I signaling through the RLRs pathway. Since IFN-I plays a vital role in antiviral
183 process, we wondered whether the stabilized caspase-1 can affect it. We initially
184 found that overexpression of caspase-1 in IPEC-J2 cells attenuated the *IFN-α*, *IFN-β*,
185 *ISG15* and *OAS1* mRNA levels induced by poly (I:C) treatment (Fig. 3A-D). In
186 addition, caspase-1 inhibitor VX765 reversed the attenuated IFN-I signaling during
187 poly (I:C) treatment (Fig. 3E and F). Moreover, knockout of caspase-1 in THP-1 cells
188 further promoted the expression of *IFN-β* and *ISG15* mRNA induced by poly (I:C)
189 (Fig. 3G and H). Same results were observed for PLP2 in IPEC-J2 cells (Fig. 3I and J).
190 Thus, we determined that both caspase-1 and PLP2 were antagonists of IFN-I. Next,
191 the above-mentioned findings were further verified in PEDV-infected IPEC-J2 cells,
192 which were consistent with our observations (Fig. 3 K-P). These results indicate that
193 PEDV-induced IFN-I signaling was counteracted by the stabilized caspase-1.

194 The role of caspase-1 and PLP2 in viral replication was further analyzed
195 considering the vital antiviral effect of IFN-I. PLP2 was transfected into IPEC-J2 cells
196 and then infected with PEDV. Consistent with its antagonistic effect on IFN-I, the
197 results showed that PLP2 could promote PEDV replication, which was also confirmed
198 by immunoblotting (Fig. 3Q). Since the high expression of caspase-1 leads to
199 autoprocessing, we transfected caspase-1 with different doses and then treated with
200 PEDV infection. As shown in Fig. 3R, all doses of caspase-1 could promote PEDV

201 replication, while the effect of high concentration of caspase-1 was attenuated, which
202 might relate to pyroptosis caused by caspase-1 activation. Moreover, the use of
203 VX765 inhibited viral replication co-treated with necrosulfonamide (NSA), a specific
204 GSDMD inhibitor (Fig. 3S). Together, these data suggest that the enhanced caspase-1
205 stabilized by PEDV infection attenuates type I IFN signaling and thus benefits to viral
206 replication.
207
208 **Cleavage of RIG-I by caspase-1 ensures PEDV replication**
209 As caspase-1 is vital to suppress type I IFN during PEDV infection, we hypothesized
210 that caspase-1 exerted its effect on RIG-I. Therefore, we analyzed whether caspase-1
211 could directly interact with RIG-I. HEK293T cells were then transfected with
212 MYC-tagged RIG-I and FLAG-tagged caspase-1, Co-IP assay showed that RIG-I
213 interacted with caspase-1 (Fig. 4A). Interestingly, we found that RIG-I was
214 diminished after co-transfected with caspase-1 (Fig. 4B). Thus, we co-transfected
215 caspase-1 or its mutant with RIG-I at different doses in HEK293T, followed with
216 immunoblotting. As shown in Fig. 4C, a clear band with a molecular weight around
217 25-35 kDa was observed, while the caspase-1-C285A (caspase-1 mutant) impaired the
218 cleavage. Because RIG-I was N-terminal MYC-tagged, we speculated that caspase-1
219 cut RIG-I at N-terminus. We therefore generated mutants of RIG-I at different sites to
220 identify the exact cleavage site of RIG-I by caspase-1. RIG-I or its mutants (D163A,
221 D189A, D194A, D199/202/203A and D209A) were co-transfected with caspase-1 in
222 HEK293T cells. As shown in Fig. 4D and Supplementary Fig. 3A, wild-type RIG-I,

223 D163A, D194A, D199/202/203A and D209A could still be cleaved by caspase-1
224 successfully, while RIG-I-D189A could not be cleaved. These results imply that RIG-I
225 was a cleaved target of caspase-1 at D189. Moreover, we investigated the relationship
226 between human derived caspase-1 and RIG-I. As shown in Supplementary Fig. 3B, a
227 band with a molecular weight around 25-35 kDa was observed (lane 2). Based on the
228 multiple-sequence alignment of RIG-Is (Supplementary Fig. 3C), different mutants,
229 including single or double mutants of human RIG-I (h-RIG-I) were generated and
230 co-expressed with empty vector or h-caspase-1. The results showed that the cleaved
231 fragments from all of the mutants were reduced compared to the wild type RIG-I
232 (Supplementary Fig. 3B). We next generated a triple mutant of RIG-I
233 (h-RIG-I-D163/194/234A) and transfected it with caspase-1 in HEK293T cells.
234 Supplementary Fig. 3D revealed that the cleaved band between 25-35 kDa was further
235 weakened, suggesting that the D163, D194 and D234 residues of RIG-I might be the
236 cleavage sites of human derived caspase-1.

237 To further investigate the effects of RIG-I cleavage on viral replication and type I
238 IFN signaling, Vero cells were transfected with empty vector (EV), RIG-I or
239 co-transfected with caspase-1 and RIG-I, followed by PEDV infection. As shown in
240 Fig. 4E, RIG-I significantly attenuated viral replication, while the co-transfected
241 group reversed this effect. We then generated a RIG-I mutant, RIG-I-D189A, and
242 transfected into IPEC-J2 cells and then infected with PEDV. As expected, wild type
243 RIG-I facilitated *IFN-β* and *ISG15* production and inhibited PEDV replication, and
244 the RIG-I-D189A mutant further enhanced IFN-I signaling and impaired viral

245 replication (Fig. 4F-H). Next, we evaluated the function of RIG-I-1-189aa and
246 RIG-I-190-943aa in activating the innate immune response as well as in viral
247 replication. We found that wild-type RIG-I promoted IFN induction and inhibited
248 PEDV replication, while RIG-I-1-189aa or RIG-I-190-943aa potently reversed IFN-I
249 production and restored viral reproduction (Fig. 4I-K). Taken together, these results
250 collectively demonstrate that caspase-1 targets the D189 residue of porcine RIG-I for
251 cleavage and the cleaved fragments lose their function to inhibit PEDV replication.
252

253 **PLP2 degrades GSDMD-p30 by removing the K27-linked ubiquitin chains at**
254 **K275 residue to inhibit pyroptosis**

255 The activation of caspase-1 can lead to GSDMD cleavage and thus cause pyroptotic
256 cell death. However, according to the above results, PEDV infection did not cause
257 substantial pyroptosis at early stage (Fig. 1H and I). To determine whether PLP2 also
258 targets GSDMD and regulates pyroptosis, HEK293T cells were initially
259 co-transfected with GSDMD-FL and caspase-1 for 6 h, and then PLP2 was transfected
260 in a dose-dependent manner. The immunoblotting results showed that the cleaved
261 fragment of GSDMD (GSDMD-p30) was decreased in the presence of PLP2 (Fig.
262 5A). Meanwhile, we repeatedly observed a reduced protein level of GSDMD-p30
263 after overexpression of PLP2, but had no variation on GSDMD-FL (Fig. 5B and
264 Supplementary Fig. 4A). The LDH release assay and the propidium iodide (PI)
265 staining also confirmed that PLP2 had an inhibitory effect on pyroptotic cell death
266 induced by GSDMD-p30 (Fig. 5C and Supplementary Fig. 4B). As shown in Fig. 5D,

267 PLP2 had a stronger interaction with GSDMD-p30 than GSDMD-FL, which further
268 demonstrated the complex relationship between GSDMD-p30 and PLP2. In order to
269 evaluate the effect of PLP2 on GSDMD-p30 more directly, we co-transfected
270 GFP-tagged PLP2 and FLAG-tagged GSDMD-p30 in HEK293T cells. GSDMD-p30
271 was found to localize mainly in the cytoplasm, formed specks and ultimately resulted
272 in rupture of the membrane (Fig. 5E top row). In the presence of PLP2, GSDMD-p30
273 was evenly dispersed in cytoplasm, failed to form pyroptotic specks (Fig. 5E bottom
274 row). Taken together, we reveal that PLP2 degrades GSDMD-p30 and thus blocks
275 pyroptosis.

276 To determine which degradation system is responsible for the degradation of
277 GSDMD-p30, we examined the effect of the proteasome inhibitor MG132, the
278 autophagy inhibitor 3MA and CQ on GSDMD-p30 degradation in the presence of
279 PLP2. The results showed that PLP2-mediated degradation of GSDMD-p30 was
280 rescued by MG132, which meant that GSDMD-p30 degradation was corresponded
281 with proteasome pathway (Fig. 6A). We further revealed that all the catalytic mutants
282 of PLP2 (C113A, H272A, D285A) lost the ability to degrade GSDMD-p30 which was
283 also confirmed by the LDH release assay (Fig.6B and C), suggesting that the
284 deubiquitinase activity of PLP2 is essential for the GSDMD-p30 degradation. To
285 determine the lysine residues of GSDMD-p30 to which ubiquitin is attached, we used
286 the UbPred program (http://www.ubpred.org), to predict the potential ubiquitination
287 sites of porcine GSDMD-p30. This analysis revealed three putative lysine residues:
288 K103, K177 and K275. We then generated GSDMD-p30-K103R, K177R and K275R

289 mutants in which each of these lysine residues was replaced with arginine (R). We
290 co-transfected the wild type porcine GSDMD-p30 and three of its mutants with
291 HA-tagged ubiquitin, followed with immunoblotting. As shown in Fig. 6D,
292 co-transfection of HA-Ub failed to promote GSDMD-p30-K275R mutant
293 ubiquitination, suggesting that Lys275 residue might be the ubiquitination site of
294 GSDMD-p30. Next, we co-transfected HA-tagged ubiquitin mutants (with only one of
295 the seven lysine residues retained as lysine, while the other six replaced with arginine)
296 with GSDMD-p30 in HEK293T cells. The LDH release assay revealed that
297 K27-linked ubiquitin mutant markedly elevated the LDH level (Fig. 6E), which was
298 consistent with our previous study[26]. Ubiquitination assay further confirmed that
299 K27-linked ubiquitin promoted the ubiquitination of GSDMD-p30 (Fig. 6F, lane 2
300 and 4) and K275R mutant displayed a significant reduction of K27-linked
301 ubiquitination (Fig. 6F, lane 4 and 5). Moreover, we co-expressed the wild type PLP2
302 or its mutants with HA-tagged K27-linked ubiquitin and FLAG-tagged GSDMD-p30
303 and then performed Co-IP assay. As expected, wild type PLP2 dramatically reduced
304 K27-linked ubiquitination of GSDMD-p30, while neither of its mutants performed the
305 same effect (Fig. 6G). To further confirm the role of K275 residue of GSDMD, we
306 designed three siRNAs targeting porcine GSDMD. The efficiency of GSDMD
307 knockdown in IPEC-J2 cells was shown in Supplementary Fig. 4C, and we selected
308 si-GSDMD#1 for further studies. IPEC-J2 cells were transfected with GSDMD-FL or
309 GSDMD-FL-K275R upon siRNA-mediated knockdown of GSDMD, followed by
310 PEDV infection. As shown in Supplementary Fig. 4D, GSDMD-FL-K275R facilitated

311 the viral replication compared to wild type GSDMD-FL, the LDH assay further
312 confirmed this (Supplementary Fig. 4E). Taken together, our results demonstrate that
313 PLP2 is able to degrade GSDMD-p30 by removing the K27-linked ubiquitin chain at
314 K275 residue of GSDMD-p30 and thus abrogate pyroptosis.
315

316 **CoVs using different strategies to disrupt antiviral response and inhibit**
317 **pyroptosis**

318 Next, we tested whether papain-like proteases in other genus of CoVs have the same
319 effects on GSDMD-p30 and caspase-1. PEDV-PLP2, SARS-CoV-2-PLpro and
320 PDCoV-PLpro were generated and then transfected into HEK293T cells with
321 GSDMD-p30. As shown in Fig. 7A and B, all these papain-like proteases could inhibit
322 LDH release and degrade GSDMD-p30, which revealed their ability in abrogating
323 pyroptosis. Furthermore, we examined the role of these viral proteins in stabilizing
324 caspase-1 and found that only PEDV PLP2 could promote caspase-1 expression (Fig.
325 7C). It is possible that PDCoV and SARS-CoV-2 use different ways to activate
326 caspase-1. To evaluate the effect of these viral proteins on PEDV replication, IPEC-J2
327 cells were transfected with empty vector or these papain-like proteases, and then
328 infected with PEDV. All these papain-like proteases were able to promote viral
329 replication (Fig. 7D). Collectively, GSDMD-p30 was attenuated by papain-like
330 proteases of CoVs, which led to higher viral replication.

331 It has been reported that the nucleocapsid protein (N) of SARS-CoV-2 activates the
332 NLRP3 inflammasome, thus we hypothesized that NLRP3 inflammasome-mediated

333 caspase-1 activation could also antagonize IFN production. In that case, we generated
334 THP-1 cell lines stably expressing FLAG-EV-Lentivirus (negative control) or
335 FLAG-N-Lentivirus (Lentivirus carrying the SARS-CoV-2 N gene) (Fig. 7E).
336 Consistent with previous studies[18], FLAG-N-Lentivirus elevated the secretion of
337 IL-1β, suggesting that SARS-CoV-2 N can activate NLRP3 inflammasome (Fig. 7F).
338 To evaluate the role of SARS-CoV-2 N in IFN production, the differentiated
339 macrophages were then stimulated with poly (I:C) and we found that the endogenous
340 RIG-I was significantly reduced in the presence of SARS-CoV-2 N (Fig. 7G). As
341 shown in Fig. 7H and I, the production of IL-1β was elevated while the IFN-β was
342 dramatically reduced by SARS-CoV-2 N. Moreover, qRT-PCR analyses revealed that
343 the expression of *IFN-β* and ISG15 mRNA level were notably repressed by
344 SARS-CoV-2 N (Fig. 7J and K), indicating that the activated caspase-1 targeted
345 RIG-I to abrogate IFN-I signaling. LDH release assay also confirmed the inhibitory
346 effect of SARS-CoV-2 N on GSDMD-mediated pyroptosis (Fig. 7L). Taken together,
347 we unravel a novel antagonistic mechanism employed by different viral proteins from
348 CoVs and thus evade host IFN signaling and pyroptosis (Fig.8).
349

350 **Discussion**

351 A variety of viruses have been reported to activate inflammasomes. The
352 inflammasome operates as a platform for caspase-1 activation, resulting in
353 caspase-1-dependent IL-1β release and subsequent pyroptosis. This, in turn, increases
354 the expression of antiviral genes to control invading pathogens[27]. As a countermeasure,

355 viruses have evolved strategies to antagonize host immune response. Previous study
356 has demonstrated that DNA virus-induced inflammasome-mediated active caspase-1
357 cleaves human cGAS at D140 and D157 to dampen IFN production[25]. In the present
358 study, we demonstrated the sophisticated regulation of RNA virus to counteract IFN-I
359 signaling and pyroptosis using active caspase-1 and papain-like protease. We found
360 that CoVs-induced active caspase-1 disrupts IFN-I signaling by cleaving RIG-I to
361 produce inactive fragments. Meanwhile, papain-like protease of CoVs can degrade
362 GSDMD-p30 by removing its K27-linked ubiquitin chain at K275 residue to restrain
363 pyroptosis. Therefore, our work unravels a novel antagonistic mechanism employed
364 by CoVs to evade host antiviral response.

365 To date, most viruses induced caspase-1 activation is mediated by inflammasomes.
366 EV71 3D and ZIKV NS5 activate the NLRP3 inflammasome by interacting with
367 NACHT and the LRR domain of NLRP3[17,28,29]. NS1 of ZIKA also enhances NLRP3
368 inflammasome activation to facilitate its infection[24]. The influenza A virus (IAV)
369 non-structural protein PB1-F2 contributes to severe pathophysiology through
370 triggering NLRP3-dependent caspase-1 activation[30]. Except for NLRP3, viruses can
371 also induce other inflammasomes activation. Human rhinovirus (HRV) 3C protease
372 directly cleaves human NLRP1 between the Glu130 and Gly131 junction, which
373 liberates the activating C-terminal fragment and subsequently promoting NLRP1
374 inflammasome activation[31]. NLRP9b recognizes short double-stranded RNA stretches
375 via RNA helicase Dhx9 and forms inflammasome complexes with ASC and
376 pro-caspase-1 to promote caspase-1-dependent IL-1β release and pyroptosis[32]. Herpes

377 simplex virus 1 (HSV1) can induce AIM2-, pyrin- and ZBP1-mediated caspase-1
378 activation, cytokine release and cell death[33]. For coronaviruses, studies have shown
379 that MERS-CoV and at least three different proteins of SARS-CoV-2 can induce
380 NLRP3 inflammasome activation and caspase-1-mediated subsequent
381 pyroptosis[18,20,34,35]. Evidence also demonstrated that circulating monocytes from
382 COVID-19 patients show signs of AIM2 inflammasome activation and
383 caspase-1-meidated GSDMD cleavage and pyroptosis[21]. Unlike the reported manner
384 of caspase-1 activation, our results suggest that PEDV induces porcine caspase-1
385 activation via its papain-like protease PLP2 through elevating pro-caspase-1
386 expression by removing its K11-linked ubiquitin chains at K134 residue. Studies have
387 demonstrated that accumulated pro-caspase-1 lead to autoprocessing within the
388 catalytic domain[11-13]. Consequently, active caspase-1 targets to porcine RIG-I for
389 cleavage at D189 residue leading to decreased IFN-I signaling and enhanced PEDV
390 replication. Interestingly, PLPro from SARS-CoV-2 and PDCoV did not use this way
391 to activate caspase-1, as they can trigger NLRP3- or AIM2-mediated caspase-1
392 activation. Similarly, inflammasome-mediated caspase-1 activation also cleaved
393 human RIG-I to abrogate IFN-I signaling pathway. Therefore, our study suggests that
394 the main purpose of virus-induced inflammasome-mediated caspase-1 activation is to
395 antagonize IFN-I signaling. A newly published study further indicated that
396 SARS-CoV-2 infection induced high expression of pro-caspase-4/11, which may
397 result in its auto-activation in the absence of a ligand[36]. Thus, our results uncover a
398 new and different mechanism of CoVs inducing caspase-1 activation.

399 Activation of inflammasome is often vital in the host antiviral immune
400 response[35,37-39]. It is obvious that triggering of pyroptosis and inflammasomes
401 activation is detrimental to the replication and survival of viruses. Thus, viruses have
402 also developed strategies to antagonize extensive inflammasome activation and
403 pyroptosis, especially at the early stage of viral infection. The human papillomavirus
404 (HPV) oncoprotein E7 promotes the TRIM21-mediated K33-linked ubiquitination of
405 the IFI16 inflammasome for degradation to inhibit pyroptosis. African swine fever
406 virus (ASFV) pS273R cleaves GSDMD at G107-A108 to generate a shorter
407 N-terminal of GSDMD (GSDMD-N_{1-107}) which is not capable of triggering pyroptosis.
408 The accessory protein (PB1-F2) of H5N1 and H3N2 influenza A viruses (IAV) can
409 bind to the pyrin and LRR domains of NLRP3 and prevent NEK7 binding to stabilize
410 the auto-repressed and closed conformation of NLRP3. 2A and 3C proteases of EV71
411 can cleave NLRP3 directly to inhibit the activation of inflammasome, while the EV71
412 3C-like protease can also cleave GSDMD to block the pyroptosis pathway. Our recent
413 research also proved that 3C-like proteases Nsp5 of coronaviruses (PEDV, PDCoV,
414 SARS-CoV-2 and MERS-CoV) can cleave GSDMD at Q193 to produce two
415 fragments that are unable to trigger pyroptosis. SARS-CoV-2 N induces
416 pro-inflammatory cytokines through promoting the assembly and activation of the
417 NLRP3 inflammasome[18]. However, SARS-CoV-2 N protein is also capable of
418 binding to GSDMD directly to inhibit the GSDMD cleavage from caspase-1 to avoid
419 pyroptosis[40]. Our results demonstrated that SARS-CoV-2 N-induced NLRP3
420 inflammasome activation can antagonize IFN production through cleaving RIG-I by

activated caspase-1. In the present study, we further demonstrated that CoVs (PEDV, PDCoV and SARS-CoV-2) can abrogate pyroptosis by degradation of GSDMD-p30 via their papain-like proteases. Therefore, we discovered a novel mechanism for CoVs to antagonize pyroptosis.

In conclusion, we used PEDV as a model of CoVs to illustrate the sophisticated regulation of CoVs to counteract IFN-I signaling and pyroptosis. For the first time, we demonstrate the role of inflammasome dependent or independent caspase-1 activation in antagonizing IFN-I signaling. Furthermore, we show that papain-like protease of CoVs can inhibit pyroptosis by degradation of GSDMD-p30 through proteasome pathway. Thus, our present study unveils a novel antagonistic mechanism by which CoVs manipulates the cross-talk of IFN signaling and pyroptosis, which might indicate a framework for design of anti-CoVs therapies.

Methods

Reagents and antibodies

Anti-HA (3724) and anti-Caspase-1 (2225) antibodies were purchased from Cell Signaling Technology. Anti-FLAG antibody (F1804), anti-MYC antibody (C3956) and anti-FLAG magnetic beads (10004D) were obtained from Sigma. Anti-FLAG antibody (rabbit source), Goat pAb to MS IgG (Chromeo 546, ab60316), Dnk pAb to Rb IgG (Alexa Fluor 647, ab150075) fluorescent secondary antibodies were acquired from Abcam. Anti-GAPDH antibody, HRP-labeled goat anti-rabbit IgG and goat anti-mouse IgG were from Hangzhou Fudebio. Anti-GSDMDC1 antibody (sc-393581)

443 was purchased from Santa Cruz. Anti-RIG-I antibody (20566) was obtained from
444 proteintech. The anti-PEDV N monoclonal antibody was prepared in our laboratory as
445 previously described[41]. Efficient eukaryotic transfection reagent VigoFect was
446 obtained from Vigorous Biotechnology (Beijing), Lipo8000TM transfection reagent
447 was obtained from Beyotime Biotechnology while Lipofectamine 2000 transfection
448 reagent was obtained from Invitrogen.

449 **Plasmids**

450 Eukaryotic expression vectors used in this subject were saved in our laboratory. The
451 PLP2 fragment sequence was amplified from cDNA of PEDV strain ZJ15XS0101
452 (GenBank accession no. KX55SO0281) which was isolated by our collaborating
453 laboratories for generational preservation, while amplification of the porcine GSDMD
454 gene and the porcine caspase-1 gene used cDNA of IPEC-J2 as a templet. The PLP2
455 gene was cloned to PRK-MYC vector, and the porcine GSDMD gene was cloned onto
456 p3×FLAG-CMV vector. The porcine caspase-1 gene was cloned to PCMV-HA and
457 p3×FLAG-CMV vector, respectively. Porcine GSDMD-p30 fragment was amplified
458 from the p3×FLAG-N-GSDMD-FL plasmid and cloned onto p3×FLAG-CMV. PLP2,
459 caspase-1 and GSDMD-p30 enzyme active site mutants were constructed based on
460 the eukaryotic expression plasmids PRK-MYC-PEDV-PLP2, HA-PCMV-Caspase-1
461 and p3×FLAG-GSDMD-p30. The plasmids encoding SARS-CoV-2 PLPro, PDCoV
462 PLPro and SARS-CoV-2-N were synthesized by Tsingke Biotech. Primers used in the
463 plasmids construction are listed in table 1 in supplementary materials.

464 **Cell culture and transfection**

465 IPEC-J2 cells, Vero cells and HEK293T cells were cultured in Dulbecco's modified
466 Eagle's medium (DMEM) with added 10% FBS and 1% penicillin-streptomycin. Wild
467 type THP-1 and caspase-1 deficient THP-1 were cultured in PRIM 1640 medium
468 containing 10% FBS and 1% penicillin-streptomycin solution. The PEDV strain
469 ZJ15XS0101 (GenBank accession no. KX55SO0281) was isolated and stored in our
470 laboratory[42]. When HEK293T cells seeded in plates grow to about a density of
471 60%~80%, indicated plasmids were transfected to the cells by VigoFect according to
472 the manufacturer's operation guide. When IPEC-J2 and Vero seeded in plates grow to
473 approximately 70%~80%, they were transfected with corresponding plasmids using
474 Lipo8000 transfection reagent according to the manufacturer's introduction. Lipo2000
475 was applied in the transfection of poly(I:C) (Merck) to IPEC-J2 during the second
476 transfection period.

477 **Viral infection**

478 Viral infection was performed when the IPEC-J2 or Vero cells grow to the density
479 around 80%~90% or after the transfection of other indicated plasmids.

480 **Lentivirus infection**

481 *SARS-COV-2-N* over-expressing THP-1 cells were generated using lentiviral infection
482 technique. After cloning *SARS-COV-2-N* coding sequence to the
483 pLVX-IRES-Puro-3×Flag lentiviral vector plasmid, HEK293T cells were
484 co-transfected with pLVX-IRES-Puro-3×Flag-SARS-COV-2-N, pMD2G and
485 PSPAX2. Supernatant was collected after 48 h incubation for further lentiviral
486 concentration.

487 **Inhibitors treatment**

488 The caspase-1 specific inhibitor VX765 diluted to 20 μM was used after plasmid
489 transfection, during viral infection or before poly(I:C) transfection. Protein synthesis
490 inhibitor cycloheximide (CHX) diluted to 25 μg/ml was added at different time points
491 before receiving samples. Fresh culture medium containing proteasome inhibitor
492 MG132, autophagy initiation inhibitor 3MA or autophagy lysosome inhibitor CQ of
493 appropriate concentration were added to different wells of cell-culturing plates 6 h
494 before receiving samples.

495 **Cytotoxicity assay**

496 Cells transfected with corresponding plasmids for 24 h were applied to cytotoxicity
497 test using CytoTox 96® Reagent (Promega) according to the manufacturer's manual.
498 OD values were read at 492 nm on an enzyme marker (Thermo Scientific).

499 **Immunoblotting**

500 Total proteins were extracted from cells lysed by RIPA lysis buffer (Beyotime
501 Biotechnology) supplemented with 1% Phenylmethanesulfonyl fluoride (PMSF)
502 (Beyotime Biotechnology). After being separated on the 10% SDS-PAGE gel (Verde
503 Biotechnology), protein stripes were transferred onto the polyvinylidene difluoride
504 (PVDF) membranes (Bio-rad). Membranes were blocked in the blocking buffer
505 (Beyotime Biotechnology), followed by incubation with primary antibodies and
506 positioning with secondary antibodies. Chemiluminescent signals were captured by an
507 ECL chemiluminescence imaging analysis system (Clinx Science Instruments).

508 **Co-immunoprecipitation**

509 Cells were lysed using IP lysis buffer (Beyotime Biotechnology) for 15 min at 4℃,
510 and then centrifuged at speed 10000 rpm at 4℃ for 15 min. After being incubated
511 with the supernatant of the cell lysis solution in a flip mixer (Kylin-Bell) overnight,
512 the magnetic beads coated with FLAG-antibodies (sigma) were washed with
513 coIP-buffer for 5 times. Soaking in 1×loading buffer, magnetic beads absorbed with
514 target proteins were denatured for 10 min in a boiling water bath. After discarding
515 magnetic beads, the remaining protein samples were applied to subsequent
516 immunoblotting assay.

517 **Confocal immunofluorescence assay**

518 HEK293T cells were seeded on glass slides placed in 24-well plates. After being
519 transfected for 24 h, cells were fixed with Immunol Staining Fix Solution (Beyotime),
520 permeabilized with Immunostaining Permeabilization Solution with Saponin
521 (Beyotime), blocked with QuickBlock Blocking Buffer for Immunol Staining
522 (Beyotime), and then incubated with indicated antibodies. The cells were observed
523 under a laser confocal microscope (Olympus).

524 **ELISA**

525 Supernatants collected from transfected cells were applied to the detection of IL-1β
526 and IFN-β according to the manufacturer's instructions. Each trial group was
527 conducted independently for three times.

528 **Total RNA extraction and reverse transcription**

529 Add RNA-easy Isolation Reagent (Vazyme Biotechnology) to cells to gather lysis
530 solution containing cells. Follow the manufacturer's introduction to extract the RNA.

531 After measuring the product RNA concentration, use the HiScript III RT SuperMix for
532 qPCR (+gDNA wiper) (Vazyme Biotechnology) to reverse transcribe RNA to cDNA.

533 **Quantitative real-time polymerase chain reaction (qRT-PCR)**

534 qRT-PCR was performed with ChamQ Universal SYBR qPCR Master Mix (Vazyme
535 Biotechnology) according to the manufacturer's requirements. Primers demanded in
536 this analysis were listed in table 2 in supplementary materials.

537 **RNA interference**

538 SiRNAs (Genepharma) specific for porcine GSDMD were transfected into IPEC-J2
539 cells using the Lipofectamine 8000 transfection reagent according to the
540 manufacturer's instructions. The sequences of GSDMD siRNAs were listed in table 3
541 in supplementary materials.

542 **Propidium iodide staining**

543 Cells were incubated with Propidium iodide (PI) (BD Bioscience) for 15 min under
544 light-proof conditions after transfection with indicated plasmids for 24 h. Dyeing
545 condition was observed under fluorescence microscope (Nikon).

546 **Statistical analysis**

547 All experiments were performed independently at least three times. Data were
548 presented as the mean ± standard deviation (SD), analyzed and used for statistical
549 graphing by GraphPad Prism 8, the significance of differences was determined by
550 One-way ANOVA or Student's *t*-test. The significance of differences ranked as:
551 ****stands for P<0.0001, ***stands for P<0.001, ** stands for P<0.01, * stands for
552 P<0.05 and ns stands for non-significant difference.

Data availability

The authors declare that all data supporting the findings of this article are available within the paper and the supplementary information files or are available from the authors upon request.

References

1. Zhang, Q. & Yoo, D. Immune evasion of porcine enteric coronaviruses and viral modulation of antiviral innate signaling. *Virus Res* **226**, 128-141 (2016).
2. Stevenson, G.W. *et al.* Emergence of Porcine epidemic diarrhea virus in the United States: clinical signs, lesions, and viral genomic sequences. *J Vet Diagn Invest* **25**, 649-654 (2013).
3. Jung, K. & Saif, L.J. Porcine epidemic diarrhea virus infection: Etiology, epidemiology, pathogenesis and immunoprophylaxis. *Vet J* **204**, 134-143 (2015).
4. Xing, Y. *et al.* The papain-like protease of porcine epidemic diarrhea virus negatively regulates type I interferon pathway by acting as a viral deubiquitinase. *J Gen Virol* **94**, 1554-1567 (2013).
5. Chu, H.F. *et al.* Structural and Biochemical Characterization of Porcine Epidemic Diarrhea Virus Papain-Like Protease 2. *J Virol* **96**, e0137221 (2022).
6. Clementz, M.A. *et al.* Deubiquitinating and interferon antagonism activities of coronavirus papain-like proteases. *J Virol* **84**, 4619-4629 (2010).
7. Zheng, D., Chen, G., Guo, B., Cheng, G. & Tang, H. PLP2, a potent deubiquitinase from murine hepatitis virus, strongly inhibits cellular type I interferon production. *Cell Res* **18**, 1105-1113 (2008).
8. Wang, Y. *et al.* Porcine transmissible gastroenteritis virus inhibits NF-kappaB activity via nonstructural protein 3 to evade host immune system. *Virol J* **16**, 97 (2019).
9. Man, S.M. & Kanneganti, T.D. Converging roles of caspases in inflammasome activation, cell death and innate immunity. *Nat Rev Immunol* **16**, 7-21 (2016).
10. Ball, D.P. *et al.* Caspase-1 interdomain linker cleavage is required for pyroptosis. *Life Sci Alliance* **3** (2020).
11. Boucher, D. *et al.* Caspase-1 self-cleavage is an intrinsic mechanism to terminate inflammasome activity. *J Exp Med* **215**, 827-840 (2018).
12. Ross, C. *et al.* Inflammatory Caspases: Toward a Unified Model for Caspase Activation by Inflammasomes. *Annu Rev Immunol* **40**, 249-269 (2022).
13. Bambouskova, M. *et al.* Itaconate confers tolerance to late NLRP3 inflammasome activation. *Cell Rep* **34**, 108756 (2021).
14. Jorgensen, I. & Miao, E.A. Pyroptotic cell death defends against intracellular pathogens. *Immunol Rev* **265**, 130-142 (2015).

591 15. Liu, X. *et al.* Inflammasome-activated gasdermin D causes pyroptosis by forming
592 membrane pores. *Nature* **535**, 153-158 (2016).
593 16. Sborgi, L. *et al.* GSDMD membrane pore formation constitutes the mechanism of
594 pyroptotic cell death. *EMBO J* **35**, 1766-1778 (2016).
595 17. Wang, W. *et al.* Zika virus infection induces host inflammatory responses by facilitating
596 NLRP3 inflammasome assembly and interleukin-1beta secretion. *Nat Commun* **9**, 106
597 (2018).
598 18. Pan, P. *et al.* SARS-CoV-2 N protein promotes NLRP3 inflammasome activation to
599 induce hyperinflammation. *Nat Commun* **12**, 4664 (2021).
600 19. Ahn, M. *et al.* Dampened NLRP3-mediated inflammation in bats and implications for a
601 special viral reservoir host. *Nat Microbiol* **4**, 789-799 (2019).
602 20. Jiang, Y. *et al.* Complement Receptor C5aR1 Inhibition Reduces Pyroptosis in
603 hDPP4-Transgenic Mice Infected with MERS-CoV. *Viruses* **11** (2019).
604 21. Junqueira, C. *et al.* SARS-CoV-2 infects blood monocytes to activate NLRP3 and AIM2
605 inflammasomes, pyroptosis and cytokine release. *Res Sq* (2021).
606 22. Tsu, B.V. *et al.* Diverse viral proteases activate the NLRP1 inflammasome. *Elife* **10** (2021).
607 23. Shi, F. *et al.* Coronaviruses Nsp5 Antagonizes Porcine Gasdermin D-Mediated Pyroptosis
608 by Cleaving Pore-Forming p30 Fragment. *mBio*, e0273921 (2022).
609 24. Zheng, Y. *et al.* Zika virus elicits inflammation to evade antiviral response by cleaving
610 cGAS via NS1-caspase-1 axis. *EMBO J* **37** (2018).
611 25. Wang, Y. *et al.* Inflammasome Activation Triggers Caspase-1-Mediated Cleavage of
612 cGAS to Regulate Responses to DNA Virus Infection. *Immunity* **46**, 393-404 (2017).
613 26. Shi, Y. *et al.* E3 ubiquitin ligase SYVN1 is a key positive regulator for GSDMD-mediated
614 pyroptosis. *Cell Death Dis* **13**, 106 (2022).
615 27. Shrivastava, G., Leon-Juarez, M., Garcia-Cordero, J., Meza-Sanchez, D.E. &
616 Cedillo-Barron, L. Inflammasomes and its importance in viral infections. *Immunol Res* **64**,
617 1101-1117 (2016).
618 28. Wang, W. *et al.* EV71 3D Protein Binds with NLRP3 and Enhances the Assembly of
619 Inflammasome Complex. *PLoS Pathog* **13**, e1006123 (2017).
620 29. He, Z. *et al.* NLRP3 Inflammasome Activation Mediates Zika Virus-Associated
621 Inflammation. *J Infect Dis* **217**, 1942-1951 (2018).
622 30. McAuley, J.L. *et al.* Activation of the NLRP3 inflammasome by IAV virulence protein
623 PB1-F2 contributes to severe pathophysiology and disease. *PLoS Pathog* **9**, e1003392
624 (2013).
625 31. Robinson, K.S. *et al.* Enteroviral 3C protease activates the human NLRP1 inflammasome
626 in airway epithelia. *Science* **370** (2020).
627 32. Zhu, S. *et al.* Nlrp9b inflammasome restricts rotavirus infection in intestinal epithelial cells.
628 *Nature* **546**, 667-670 (2017).
629 33. Lee, S. *et al.* AIM2 forms a complex with pyrin and ZBP1 to drive PANoptosis and host
630 defence. *Nature* **597**, 415-419 (2021).
631 34. Sun, X. *et al.* SARS-CoV-2 non-structural protein 6 triggers NLRP3-dependent
632 pyroptosis by targeting ATP6AP1. *Cell Death Differ* **29**, 1240-1254 (2022).
633 35. Lee, S., Channappanavar, R. & Kanneganti, T.D. Coronaviruses: Innate Immunity,
634 Inflammasome Activation, Inflammatory Cell Death, and Cytokines. *Trends Immunol* **41**,

1083-1099 (2020).
36. Eltobgy, M.M. *et al.* Caspase-4/11 exacerbates disease severity in SARS-CoV-2 infection by promoting inflammation and immunothrombosis. *Proc Natl Acad Sci U S A* **119**, e2202012119 (2022).
37. Kanneganti, T.D. *et al.* Bacterial RNA and small antiviral compounds activate caspase-1 through cryopyrin/Nalp3. *Nature* **440**, 233-236 (2006).
38. Kanneganti, T.D. *et al.* Critical role for Cryopyrin/Nalp3 in activation of caspase-1 in response to viral infection and double-stranded RNA. *J Biol Chem* **281**, 36560-36568 (2006).
39. Thomas, P.G. *et al.* The intracellular sensor NLRP3 mediates key innate and healing responses to influenza A virus via the regulation of caspase-1. *Immunity* **30**, 566-575 (2009).
40. Ma, J. *et al.* SARS-CoV-2 nucleocapsid suppresses host pyroptosis by blocking Gasdermin D cleavage. *EMBO J* **40**, e108249 (2021).
41. Shan, Y. *et al.* Nucleocapsid protein from porcine epidemic diarrhea virus isolates can antagonize interferon-lambda production by blocking the nuclear factor-kappaB nuclear translocation. *J Zhejiang Univ Sci B* **19**, 570-580 (2018).
42. Zhou, Y. *et al.* Effect of route of inoculation on innate and adaptive immune responses to porcine epidemic diarrhea virus infection in suckling pigs. *Vet Microbiol* **228**, 83-92 (2019).

Acknowledgements

This work was financially supported by the National Natural Science Foundation of China (32072817), the Zhejiang Provincial Key R&D Program of China (2021C02049), the Scientific Research Fund of Zhejiang Provincial Education Department (Y202045613, Y202148324), the Zhejiang Provincial Natural Science Foundation of China (LY18C180001, LY21C180001), and the Intergovernmental Collaborative Project in S & T Innovation under the National Key R & D Program (Grant No. 2018YFE0111700).

Author contributions

X.F., Y.Y., W.X. and F.S. contributed to the design of experiments and performed most

667 of the experiments. D.L, X.L., N.C., Q.L. and Y.S. performed some experiments. X.F,
668 D.L., W.X., X.L. and F.S. contributed to data analysis. X.F., D.L., Y.Y. and F.S.
669 contributed to writing the manuscript.
670

671 ## Competing interests

672 The authors declare no competing interests.
673

674 ## Figure legends

675 **Figure 1. PEDV infection elevates the expression of caspase-1. A** The intestinal
676 tissue lysates were extracted from healthy or PEDV naturally-infected piglets for
677 immunoblotting (IB). **B, C** IPEC-J2 cells were mock infected or infected with PEDV
678 at an MOI of 0.5, followed by cycloheximide (CHX) treatment (25 μg/ml) for 6 h.
679 The indicated gene mRNA was quantified by qRT-PCR (**B**). The indicated proteins
680 were analyzed by immunoblotting (**C**). **D** Vero cells were transfected with plasmid
681 encoding porcine caspase-1. At 24 h after transfection, the cells were mock infected or
682 infected with different doses of PEDV for another 24 h, the cell lysates were then
683 processed for immunoblotting. **E** Vero cells were transfected with plasmid encoding
684 porcine caspase-1. At 24 h after transfection, the cells were mock infected or infected
685 with PEDV at an MOI of 0.1. At indicated time points after infection, the cell lysates
686 were analyzed by immunoblotting. **F, H** Vero cells were co-transfected with plasmids
687 encoding GSDMD-FL and caspase-1. At 12 h after transfection, the cells were mock
688 infected or infected with different doses of PEDV for another 24 h, the cell lysates

689 were processed for immunoblotting (**F**), the supernatants were collected for LDH
690 release assay (**H**). **G, I** Vero cells were co-transfected with plasmids encoding
691 GSDMD-FL and caspase-1. At 12 h after transfection, the cells were mock infected or
692 infected with PEDV at an MOI of 0.05. At indicated time points after infection, the
693 cell lysates were analyzed by immunoblotting (**G**), the supernatants were collected for
694 LDH release assay (**I**). All results shown are representative of at least three
695 independent experiments. ****stands for P<0.0001, ***stands for P<0.001, ** stands
696 for P<0.01, * stands for P<0.05 and ns stands for non-significant difference.
697
698 **Figure 2. PLP2 inhibits the proteasomal degradation of caspase-1 by removing**
699 **K11-linked ubiquitin chains at Lys134. A** HEK293T cells were co-transfected with
700 HA-caspase-1-C285A and increasing amount of MYC-PEDV-PLP2. Cell lysates were
701 analyzed by immunoblotting. **B** HEK293T cells were co-transfected with
702 HA-caspase-1-C285A together with empty vector or MYC-PEDV-PLP2 then treated
703 with cycloheximide (CHX) (25 μg/ml) for the indicated time points. Cell lysates were
704 analyzed by immunoblotting. **C** HEK293T cells were co-transfected with
705 HA-caspase-1-C285A together with wild-type PEDV PLP2 or its protease-defective
706 mutants (C113A, H272A and D285A). Cell lysates were analyzed by immunoblotting.
707 **D** Immunoprecipitation analysis of HEK293T cells expressing FLAG-caspase-1 and
708 HA-UB together with MYC-tagged empty vector, wild-type PEDV-PLP2 or its
709 mutants as indicated. Anti-FLAG immunoprecipitates were analyzed by
710 immunoblotting (IP). The expression levels of the transfected proteins were analyzed

711 by immunoblotting (INPUT). **E** HEK293T cells were co-transfected with
712 FLAG-caspase-1 or its mutant FLAG-caspase-1-K134R together with increasing
713 amount of HA-tagged K11-linked ubiquitin (HA-K11). Cell lysates were analyzed by
714 immunoblotting. **F** HEK293T cells were transfected with FLAG-caspase-1 together
715 with HA-K11 and MYC-PEDV-PLP2 as indicated. Cell lysates were analyzed by
716 immunoblotting. **G** HEK293T cells were transfected with HA-caspase-1-C285A or its
717 mutant HA-caspase-1-C285A-K134R together with MYC-tagged empty vector or
718 PEDV PLP2. Cell lysates were analyzed by immunoblotting. **H** Vero cells were
719 transfected with FLAG-caspase-1 together with HA-K11 or empty vector. At 24 h
720 after transfection, the cells were mock infected or infected with PEDV at an MOI of
721 0.05 for another 24 h. Immunoprecipitation was performed with anti-FLAG binding
722 beads and analyzed by immunoblotting. All results shown are representative of at
723 least three independent experiments.
724
725 **Figure 3. Caspase-1 attenuates IFN-I signaling during PEDV infection. A-D**
726 Relative qRT-PCR analysis of *IFN-α*, *IFN-β*, *ISG15* and *OAS1* mRNA levels in
727 IPEC-J2 cells transfected with empty vector or caspase-1 for 24 h, and then stimulated
728 with poly (I:C) (200 ng/ml) for another 12 h. **E, F** Relative qRT-PCR analysis of
729 *IFN-β* and *ISG15* mRNA levels in IPEC-J2 cells treated with VX765 (20 μM) or
730 DMSO, followed by poly (I:C) (200 ng/ml) transfection for 12 h. **G, H** Relative
731 qRT-PCR analysis of *IFN-β* and *ISG15* mRNA levels in wild type (WT) or caspase-1
732 knockout (KO) THP-1 cells transfected with poly (I:C) (200 ng/ml) for 12 h. **I, J**

733 Relative qRT-PCR analysis of *IFN-β* and *ISG15* mRNA levels in IPEC-J2 cells
734 transfected with empty vector or PEDV PLP2 for 24 h, followed with poly (I:C) (200
735 ng/ml) transfection for another 12 h. **K, L** Relative qRT-PCR analysis of *IFN-β* and
736 *ISG15* mRNA levels in IPEC-J2 cells transfected with empty vector or caspase-1 for
737 24 h, followed with PEDV infection (MOI=0.5) for another 24 h. **M, N** Relative
738 qRT-PCR analysis of *IFN-β* and *ISG15* mRNA levels in IPEC-J2 cells treated with
739 VX765 (20 μM) or DMSO, followed with PEDV infection (MOI=0.5) for 24 h. **O, P**
740 Relative qRT-PCR analysis of *IFN-β* and *ISG15* mRNA levels in IPEC-J2 cells
741 transfected with empty vector or PEDV PLP2 for 24 h, followed with PEDV infection
742 (MOI=0.5) for another 24 h. **Q** IPEC-J2 cells were transfected with empty vector or
743 PEDV PLP2 for 24 h, followed with PEDV infection at an MOI of 0.5 for another 24
744 h. The indicated gene mRNA levels were quantified by qRT-PCR and the indicated
745 proteins were analyzed by immunoblotting. **R** Relative qRT-PCR analysis of *PEDV S*
746 mRNA levels in IPEC-J2 cells transfected with empty vector or increasing amount of
747 caspase-1 for 12 h, followed with PEDV infection (MOI=0.1) for another 24 h. **S**
748 Relative qRT-PCR analysis of *PEDV S* mRNA levels in IPEC-J2 cells transfected
749 with empty vector and treated with or without VX765 (20 μM), co-treated with
750 necrosulfonamide (NSA 8 μM), followed with PEDV infection (MOI=0.1) for another
751 24 h. All results shown are representative of at least three independent experiments.
752 ****stands for P<0.0001, ***stands for P<0.001, ** stands for P<0.01, * stands for
753 P<0.05 and ns stands for non-significant difference.
754

755 **Figure 4. Cleavage of RIG-I by caspase-1 ensures PEDV replication. A** HEK293T
756 cells co-transfected with FLAG-caspase-1 and S-MYC-RIG-I (porcine derived) were
757 lysed and immunoprecipitated with anti-FLAG beads and analyzed by
758 immunoblotting. **B, C** HEK293T cells were co-transfected with S-MYC-RIG-I and
759 increasing amount of HA-caspase-1 or HA-caspase-1-C285A. Cell lysates were
760 analyzed by immunoblotting. **D** HEK293T cells were co-transfected with wild-type
761 (WT) S-MYC-RIG-I or its mutants (D163A, D189A, D194A, D199/202/203A,
762 D209A) together with empty vector or HA-caspase-1. Cell lysates were analyzed by
763 immunoblotting. **E** Vero cells were transfected with empty vector, RIG-I together with
764 or without caspase-1. At 12 h after transfection, the cells were mock infected or
765 infected with PEDV at an MOI of 0.05. The indicated gene mRNA levels were
766 quantified by qRT-PCR. **F-H** Relative qRT-PCR analysis of *PEDV S, IFN-β* and
767 *ISG15* mRNA levels in IPEC-J2 cells transfected with empty vector, RIG-I or
768 RIG-I-D189A for 24 h, followed by PEDV infection (MOI=0.5) for another 24 h. **I-K**
769 Relative qRT-PCR analysis of *PEDV S, IFN-β* and *ISG15* mRNA levels in IPEC-J2
770 cells transfected with empty vector, RIG-I, RIG-I-1-189aa or RIG-I-190-943aa for 24
771 h, followed by PEDV infection (MOI=0.5) for another 24 h. All results shown are
772 representative of at least three independent experiments. ****stands for P<0.0001,
773 ***stands for P<0.001, ** stands for P<0.01, * stands for P<0.05 and ns stands for
774 non-significant difference.
775
776 **Figure 5. PLP2 degrades GSDMD-p30 to inhibit pyroptosis. A** HEK293T cells

777 were initially co-transfected with FLAG-GSDMD-FL and HA-caspase-1. At 6 h after
778 transfection, the cells were transfected with increasing amount of MYC-PEDV-PLP2.
779 Cell lysates were analyzed by immunoblotting. **B, C** HEK293T cells were
780 co-transfected with FLAG-GSDMD-p30 and increasing amount of
781 MYC-PEDV-PLP2. Cell lysates were analyzed by immunoblotting (**B**). The
782 supernatants were collected for LDH release assay (**C**). **D** HEK293T cells
783 co-transfected with MYC-PEDV-PLP2 together with empty vector,
784 FLAG-GSDMD-FL or FLAG-GSDMD-p30 were lysed and immunoprecipitated with
785 anti-FLAG beads and analyzed by immunoblotting. **E** HEK293T cells were
786 transfected with FLAG-GSDMD-p30 and GFP-PLP2 respectively or together for 24 h,
787 and then FLAG-GSDMD-p30 cells were labeled with indicated antibodies.
788 Subcellular localization of FLAG-GSDMD-p30 (red), GFP-PLP2 (green), and DAPI
789 (blue, nucleus marker) were visualized with confocal microscopy. All results shown
790 are representative of at least three independent experiments. ****stands for P<0.0001,
791 ***stands for P<0.001, ** stands for P<0.01, * stands for P<0.05 and ns stands for
792 non-significant difference.
793
794 **Figure 6. PLP2 removes the K27-linked ubiquitin chain at K275 residue of**
795 **GSDMD-p30. A** HEK293T cells were transfected with FLAG-GSDMD-p30 together
796 with empty vector or MYC-PEDV-PLP2 then treated with DMSO, MG132 (10 μM),
797 3MA (1 mM) or CQ (40 μM) for 6 h. Cell lysates were analyzed by immunoblotting.
798 **B, C** HEK293T cells were co-transfected with FLAG-GSDMD-p30 together with

799 empty vector, wild type PLP2 or its protease-defective mutants (C113A, H272A,
800 D285A). The supernatants were collected for LDH release assay (**B**). Cell lysates
801 were analyzed by immunoblotting (**C**). **D** HEK293T cells were co-expressed with
802 FLAG-GSDMD-p30 or its mutants (K103R, K177R, K275R) together with empty
803 vector or HA-UB. Cell lysates were analyzed by immunoblotting. **E** HEK293T cells
804 were co-transfected with FLAG-GSDMD-p30 and HA-tagged WT ubiquitin or its
805 mutants (K6, K11, K27, K29, K33, K48, K63, KO). The supernatants were collected
806 for LDH release assay. **F** Co-immunoprecipitation and immunoblot analysis of
807 extracts of HEK293T cells transfected with FLAG-GSDMD-p30 or
808 FLAG-GSDMD-p30-K275R together with HA-UB or HA-K27 ubiquitin. **G**
809 Co-immunoprecipitation and immunoblot analysis of extracts of HEK293T cells
810 transfected with FLAG-GSDMD-p30 and HA-K27 ubiquitin together with empty
811 vector, wild type PLP2 or its mutants (C113A, H272A, D285A). All results shown are
812 representative of at least three independent experiments. ****stands for P<0.0001,
813 ***stands for P<0.001, ** stands for P<0.01, * stands for P<0.05 and ns stands for
814 non-significant difference.

815

816 **Figure 7. Papain-like proteases in other CoVs can also abrogate pyroptosis by**
817 **degradation of GSDMD-p30. A, B** HEK293T cells were transfected with
818 FLAG-GSDMD-p30 together with empty vector, PEDV-PLP2, SARS-CoV-2-PLPro
819 or PDCoV-PLPro. The supernatants were collected for LDH release assay (**A**). Cell
820 lysates were analyzed by immunoblotting (**B**). **C** HEK293T cells were transfected

821 with HA-caspase-1-C285A together with empty vector, PEDV-PLP2,
822 SARS-CoV-2-PLPro or PDCoV-PLPro. Cell lysates were analyzed by
823 immunoblotting. **D** IPEC-J2 cells were transfected with empty vector, PEDV-PLP2,
824 SARS-CoV-2-PLPro or PDCoV-PLPro. At 24 h after transfection, the cells were
825 infected with PEDV at an MOI of 0.1 for another 24 h. The indicated gene mRNA
826 levels were quantified by qRT-PCR (top). Cell lysates were analyzed by
827 immunoblotting (bottom). **E** Immunoblot analysis of extracts of THP-1 cells stably
828 infected with FLAG-EV-Lentivirus or FLAG-N-Lentivirus. **F** PMA-differentiated
829 THP-1 macrophages were stably infected with FLAG-EV-Lentivirus or
830 FLAG-N-Lentivirus. The supernatants were collected and analyzed by ELISA for
831 IL-1β. **G-L** PMA-differentiated THP-1 macrophages were stably infected with
832 FLAG-EV-Lentivirus or FLAG-N-Lentivirus, followed with poly (I:C) (200 ng/ml)
833 transfection for 6 h. Cell lysates were analyzed by immunoblotting (**G**). The
834 supernatants were collected and analyzed by ELISA for IL-1β (**H**), IFN-β (**I**) and for
835 LDH release assay (**L**). The mRNA levels of *IFN-β* (**J**) and *ISG15* (**K**) were
836 quantified by qRT-PCR. All results shown are representative of at least three
837 independent experiments. ****stands for P<0.0001, ***stands for P<0.001, ** stands
838 for P<0.01, * stands for P<0.05 and ns stands for non-significant difference.
839
840 **Figure 8. Mechanistic diagram of CoVs antagonizing antiviral responses and**
841 **pyroptosis.**
842

843 **Supplementary Fig. 1. PEDV PLP2 interacts with both caspase-1 and GSDMD. A**
844 Vero cells were transfected with FLAG-GSDMD-FL and then infected with PEDV at
845 an MOI of 0.05. Immunoprecipitation was performed with anti-FLAG antibody. The
846 potential GSDMD-binding viral proteins were evaluated using MS analysis. **B**
847 Co-immunoprecipitation and immunoblot analysis of extracts of HEK293T cells
848 transfected with MYC-PEDV-PLP2 together with FLAG-GSDMD-FL or
849 FLAG-tagged empty vector. **C** Co-immunoprecipitation and immunoblot analysis of
850 extracts of HEK293T cells transfected with MYC-PEDV-PLP2 together with
851 FLAG-caspase-1 or FLAG-tagged empty vector, then treated with VX765 (20 μM). **D**
852 HEK293T cells were transfected with FLAG-GSDMD-FL, GFP-PLP2 and
853 HA-caspase-1 respectively or together for 24 h, and then the cells were labeled with
854 indicated antibodies. Subcellular localization of FLAG-GSDMD-FL (cyan),
855 GFP-PLP2 (green), HA-caspase-1 (red) and DAPI (blue, nucleus marker) were
856 visualized with confocal microscopy. All results shown are representative of at least
857 three independent experiments.
858
859 **Supplementary Fig. 2. The papain-like protease 2 of PEDV inhibits proteasomal**
860 **degradation of caspase-1. A** HEK293T cells were transfected with
861 FLAG-GSDMD-FL and HA-caspase-1 together with increasing amount of
862 MYC-PEDV-PLP2. Cell lysates were analyzed by immunoblotting. **B** HEK293T cells
863 were co-transfected with FLAG-GSDMD-FL together with empty vector or
864 MYC-PEDV-PLP2 then treated with cycloheximide (CHX) (25 μg/ml) for the

865 indicated time points. Cell lysates were analyzed by immunoblotting. **C**
866 Co-immunoprecipitation and immunoblot analysis of extracts of HEK293T cells
867 transfected with FLAG-caspase-1 or FLAG-caspase-1-K134R together with HA-K11
868 ubiquitin. All results shown are representative of at least three independent
869 experiments.
870
871 **Supplementary Fig. 3. RIG-I was cleaved by caspase-1. A** (long exposure of Fig.
872 4D) HEK293T cells were co-transfected with wild-type (WT) S-MYC-RIG-I or its
873 mutants (D163A, D189A, D194A, D199/202/203A, D209A) together with empty
874 vector or HA-caspase-1. Cell lysates were analyzed by immunoblotting. **B** HEK293T
875 cells were co-transfected with wild-type (WT) h-FLAG-RIG-I or its single, double
876 mutants (D163A, D194A, D234A, D163/194A, D163/234A, D194/234A) together
877 with empty vector or H-HA-caspase-1. Cell lysates were analyzed by immunoblotting.
878 **C** Alignment of the amino acid sequence of RIG-Is from different species. **D**
879 HEK293T cells were co-transfected with wild-type (WT) h-FLAG-RIG-I or its triple
880 mutant (D163/194/234A) together with empty vector or h-HA-caspase-1. Cell lysates
881 were analyzed by immunoblotting.
882
883 **Supplementary Fig. 4. PLP2 degrades GSDMD-p30 by removing the K27-linked**
884 **ubiquitin chains at K275 residue to inhibit pyroptosis. A** HEK293T cells were
885 transfected with FLAG-GSDMD-FL together with increasing amount of
886 MYC-PEDV-PLP2. Cell lysates were analyzed by immunoblotting. **B** HEK293T cells

887 were co-transfected with FLAG-GSDMD-p30 and MYC-PEDV-PLP2, then the cells
888 were performed with propidium iodide (PI) staining analysis. **C** Immunoblot analysis
889 of extracts of IPEC-J2 cells transfected with negative control (NC) siRNA or GSDMD
890 siRNA (si-GSDMD#1, si-GSDMD#2, si-GSDMD#3). Cell lysates were analyzed by
891 immunoblotting. **D, E** IPEC-J2 cells were transfected with GSDMD siRNA
892 (si-GSDMD#1) for 24 h and then expressed with GSDMD-FL or GSDMD-FL-K275R
893 for another 24 h. The cells were then infected with PEDV at an MOI of 0.1 for 24 h.
894 The indicated gene mRNA levels were quantified by qRT-PCR (**D**). The supernatants
895 were collected for LDH release assay (**E**). All results shown are representative of at
896 least three independent experiments. ****stands for P<0.0001, ***stands for P<0.001,
897 ** stands for P<0.01, * stands for P<0.05 and ns stands for non-significant difference.

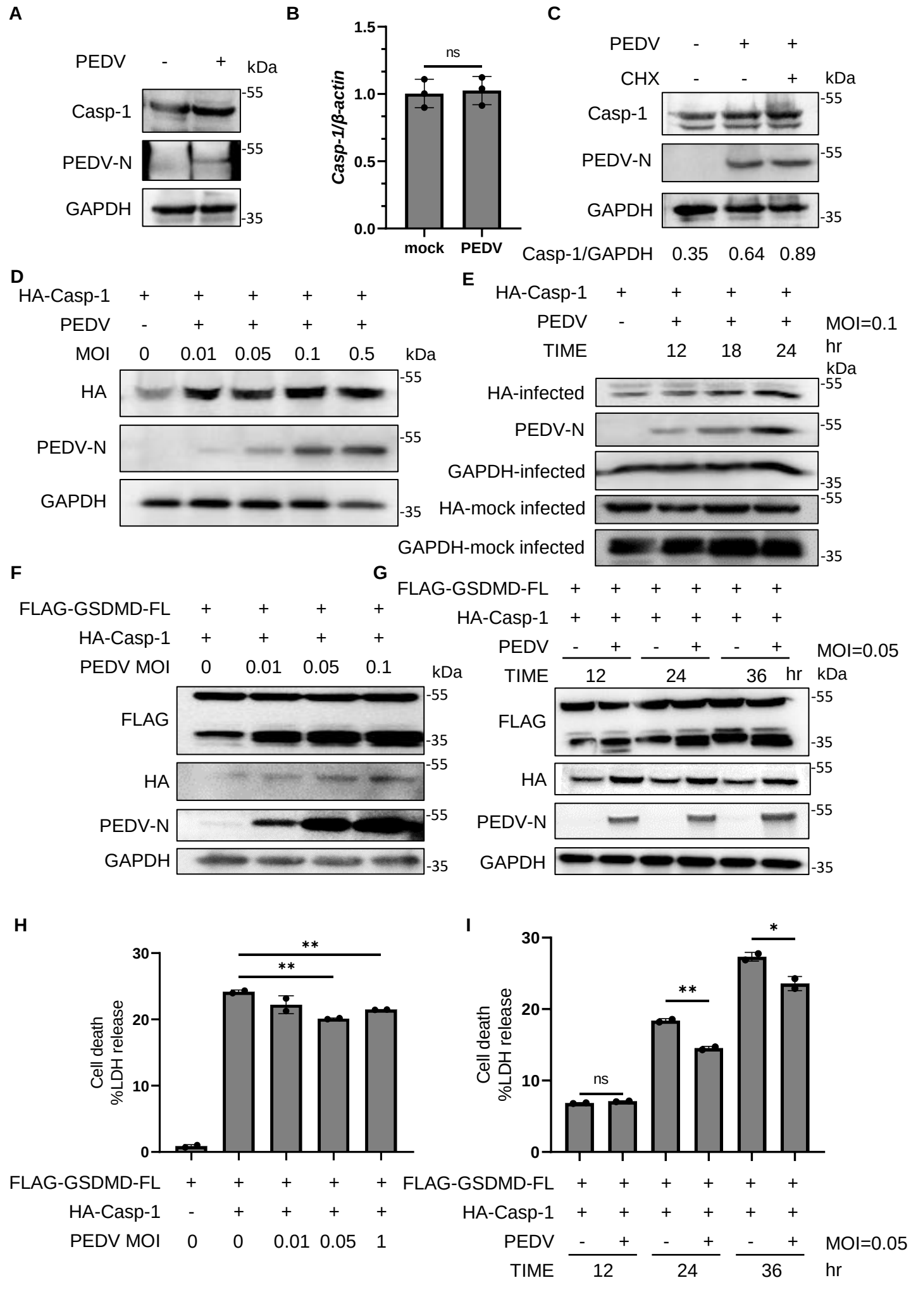
A
PEDV - +
kDa
Casp-1
PEDV-N
GAPDH
-55
-55
-35
B
Casp-1/β-actin
1.5
1.0
0.5
0.0
ns
mock
PEDV
C
PEDV - + +
CHX - - +
kDa
Casp-1
PEDV-N
GAPDH
-55
-55
-35
Casp-1/GAPDH 0.35 0.64 0.89
D
HA-Casp-1 + + + + +
PEDV - + + + +
MOI 0 0.01 0.05 0.1 0.5
kDa
HA
PEDV-N
GAPDH
-55
-55
-35
E
HA-Casp-1 + + + +
PEDV - + + + MOI=0.1
TIME 12 18 24 hr
kDa
HA-infected
PEDV-N
GAPDH-infected
HA-mock infected
GAPDH-mock infected
-55
-55
-35
-55
-35
F
FLAG-GSDMD-FL + + + +
HA-Casp-1 + + + +
PEDV MOI 0 0.01 0.05 0.1
kDa
FLAG
HA
PEDV-N
GAPDH
-55
-35
-55
-55
-35
G
FLAG-GSDMD-FL + + + + + +
HA-Casp-1 + + + + + +
PEDV - + - + - + MOI=0.05
TIME 12 24 36 hr
kDa
FLAG
HA
PEDV-N
GAPDH
-55
-35
-55
-55
-35
H
Cell death
%LDH release
30
20
10
0
**
**
FLAG-GSDMD-FL + + + + +
HA-Casp-1 - + + + +
PEDV MOI 0 0 0.01 0.05 1
I
Cell death
%LDH release
30
20
10
0
ns
**
*
FLAG-GSDMD-FL + + + + + +
HA-Casp-1 + + + + + +
PEDV - + - + - + MOI=0.05
TIME 12 24 36 hr

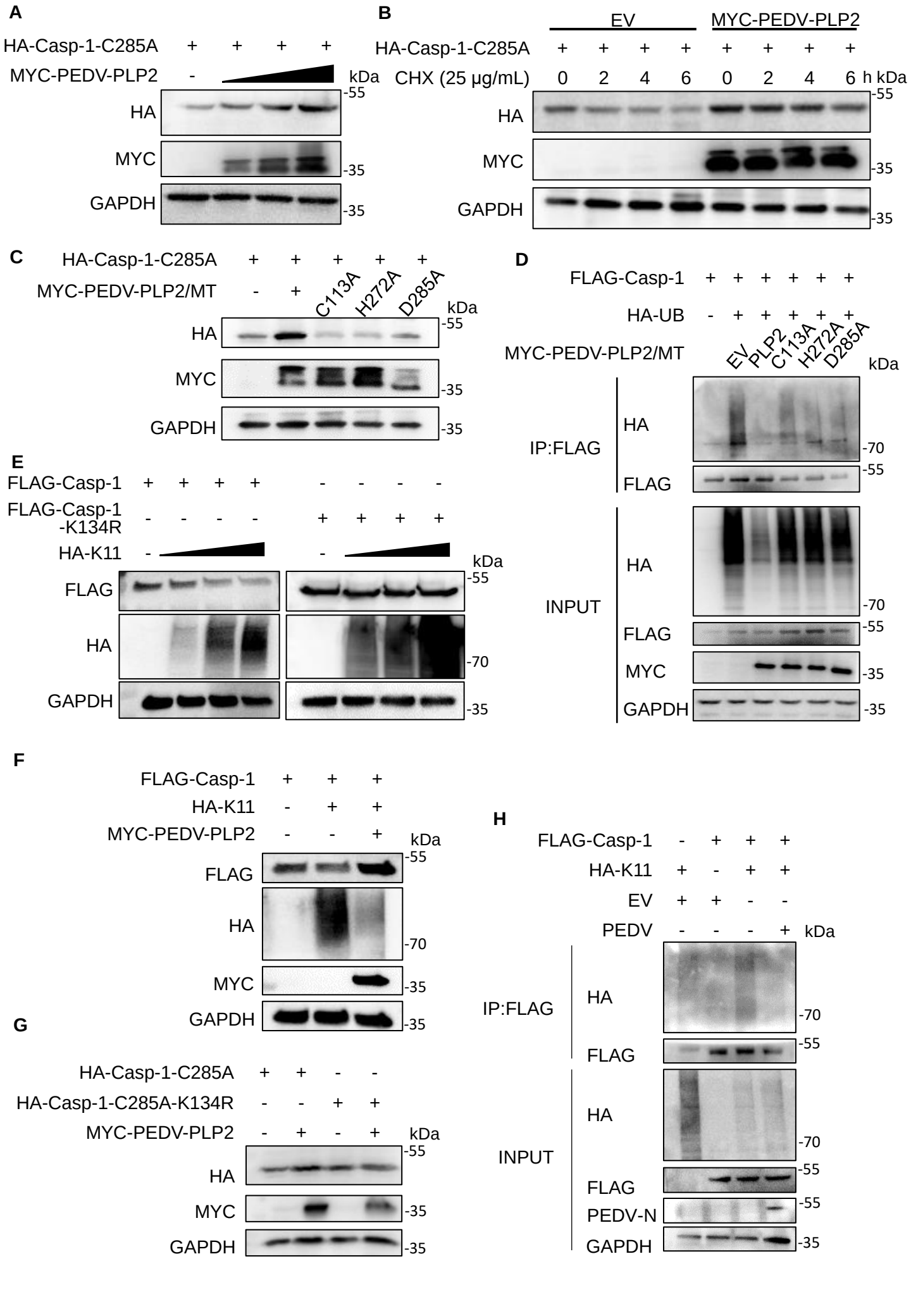
A
HA-Casp-1-C285A + + + +
MYC-PEDV-PLP2 - kDa
HA
MYC
GAPDH
-55
-35
-35
B
EV
MYC-PEDV-PLP2
HA-Casp-1-C285A + + + + + + + +
CHX (25 μg/mL) 0 2 4 6 0 2 4 6 h kDa
HA
MYC
GAPDH
-55
-35
-35
C
HA-Casp-1-C285A + + + + +
MYC-PEDV-PLP2/MT - + C113A H272A D285A kDa
HA
MYC
GAPDH
-55
-35
-35
D
FLAG-Casp-1 + + + + + +
HA-UB - + + + + +
MYC-PEDV-PLP2/MT EV PLP2 C113A H272A D285A kDa
IP:FLAG
HA
FLAG
INPUT
HA
FLAG
MYC
GAPDH
-70
-55
-70
-55
-35
-35
E
FLAG-Casp-1 + + + + - - - -
FLAG-Casp-1 -K134R - - - - + + + +
HA-K11 - - kDa
FLAG
HA
GAPDH
-55
-70
-35
F
FLAG-Casp-1 + + +
HA-K11 - + +
MYC-PEDV-PLP2 - - + kDa
FLAG
HA
MYC
GAPDH
-55
-70
-35
-35
G
HA-Casp-1-C285A + + - -
HA-Casp-1-C285A-K134R - - + +
MYC-PEDV-PLP2 - + - + kDa
HA
MYC
GAPDH
-55
-35
-35
H
FLAG-Casp-1 - + + +
HA-K11 + - + +
EV + + - -
PEDV - - - + kDa
IP:FLAG
HA
FLAG
INPUT
HA
FLAG
PEDV-N
GAPDH
-70
-55
-70
-55
-55
-35

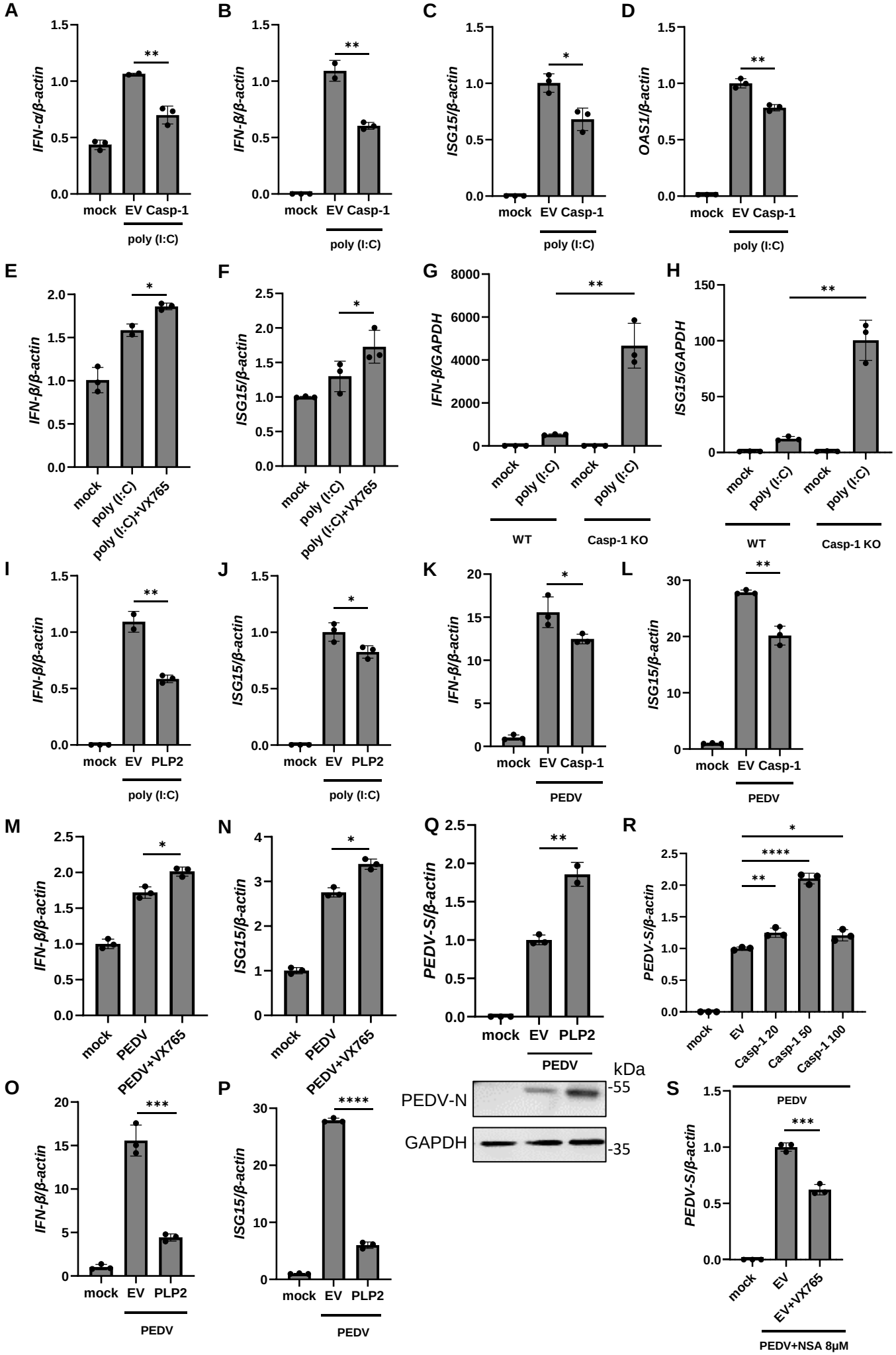
A
IFN-α/β-actin
mock
EV
Casp-1
poly (I:C)
B
IFN-β/β-actin
C
ISG15/β-actin
D
OAS1/β-actin
E
IFN-β/β-actin
poly (I:C)+VX765
F
ISG15/β-actin
G
IFN-β/GAPDH
WT
Casp-1 KO
H
ISG15/GAPDH
I
IFN-β/β-actin
PLP2
J
ISG15/β-actin
K
IFN-β/β-actin
PEDV
L
ISG15/β-actin
M
IFN-β/β-actin
PEDV
PEDV+VX765
N
ISG15/β-actin
Q
PEDV-S/β-actin
R
PEDV-S/β-actin
Casp-1 20
Casp-1 50
Casp-1 100
O
IFN-β/β-actin
P
ISG15/β-actin
kDa
PEDV-N
GAPDH
-55
-35
S
PEDV-S/β-actin
EV+VX765
PEDV+NSA 8μM

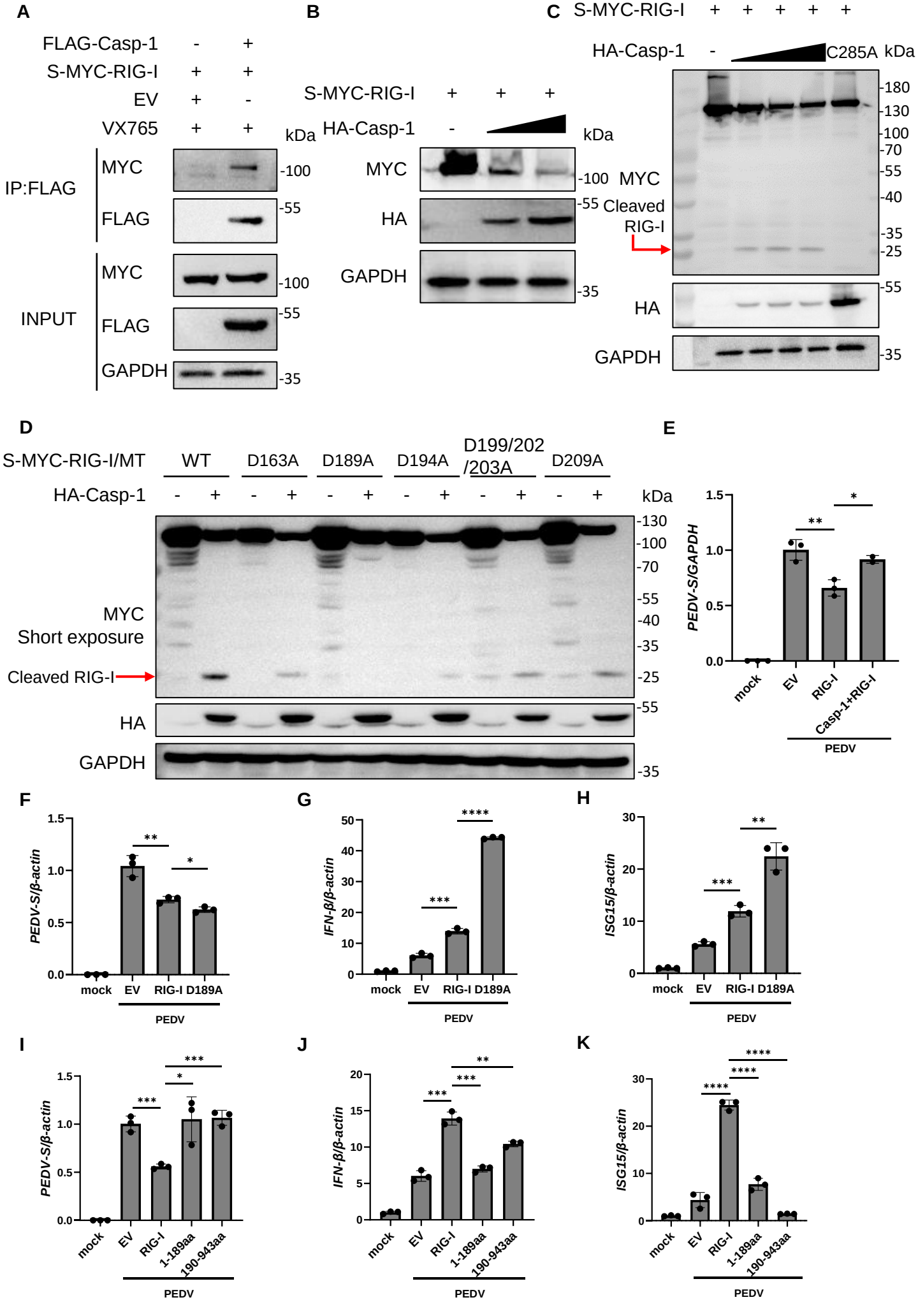
A
FLAG-Casp-1 - +
S-MYC-RIG-I + +
EV + -
VX765 + +
kDa
IP:FLAG
MYC
FLAG
INPUT
MYC
FLAG
GAPDH
-100
-55
-100
-55
-35
B
S-MYC-RIG-I + + +
HA-Casp-1 -
kDa
MYC
HA
GAPDH
-100
-55
-35
C
S-MYC-RIG-I + + + + +
HA-Casp-1 - C285A
kDa
MYC
Cleaved RIG-I
HA
GAPDH
180
130
100
70
55
40
35
25
55
35
D
S-MYC-RIG-I/MT WT D163A D189A D194A D199/202/203A D209A
HA-Casp-1 - + - + - + - + - + - +
kDa
MYC
Short exposure
Cleaved RIG-I
HA
GAPDH
130
100
70
55
40
35
25
55
35
E
PEDV-S/GAPDH
1.5
1.0
0.5
0.0
**
*
mock
EV
RIG-I
Casp-1+RIG-I
PEDV
F
PEDV-S/β-actin
1.5
1.0
0.5
0.0
**
*
mock
EV
RIG-I
D189A
PEDV
G
IFN-β/β-actin
50
40
30
20
10
0
****
***
mock
EV
RIG-I
D189A
PEDV
H
ISG15/β-actin
30
20
10
0
**
***
mock
EV
RIG-I
D189A
PEDV
I
PEDV-S/β-actin
1.5
1.0
0.5
0.0
***
*
***
mock
EV
RIG-I
1-189aa
190-943aa
PEDV
J
IFN-β/β-actin
20
15
10
5
0
**
***
***
mock
EV
RIG-I
1-189aa
190-943aa
PEDV
K
ISG15/β-actin
30
20
10
0
****
****
****
mock
EV
RIG-I
1-189aa
190-943aa
PEDV

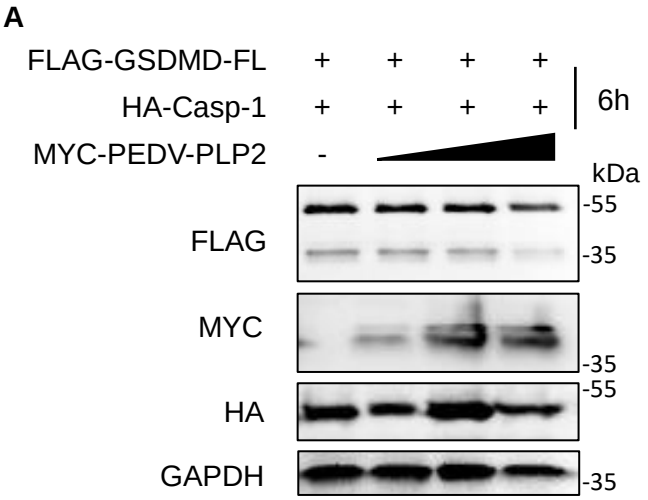
A
FLAG-GSDMD-FL + + + +
HA-Casp-1 + + + +
6h
MYC-PEDV-PLP2 -
kDa
FLAG
-55
-35
MYC
-35
HA
-55
GAPDH
-35

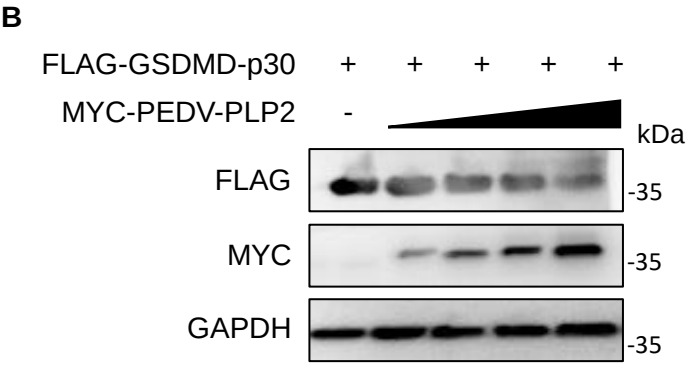
B
FLAG-GSDMD-p30 + + + + +
MYC-PEDV-PLP2 -
kDa
FLAG
-35
MYC
-35
GAPDH
-35

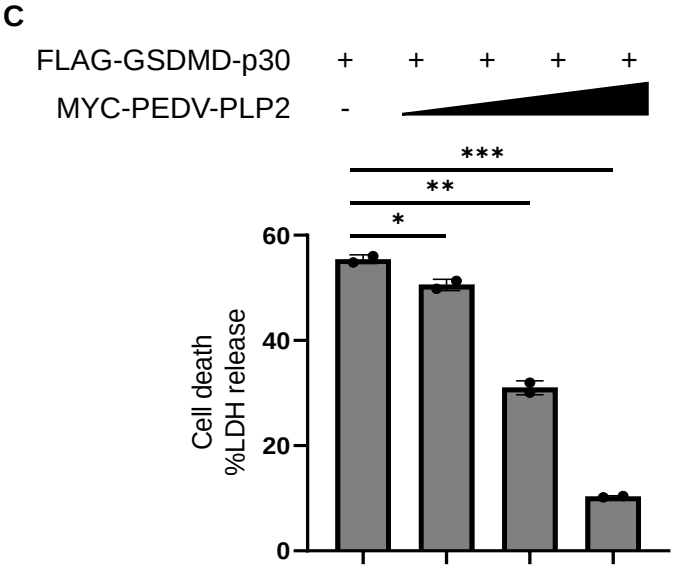
C
FLAG-GSDMD-p30 + + + + +
MYC-PEDV-PLP2 -
***
**
*
60
40
20
0
Cell death
%LDH release

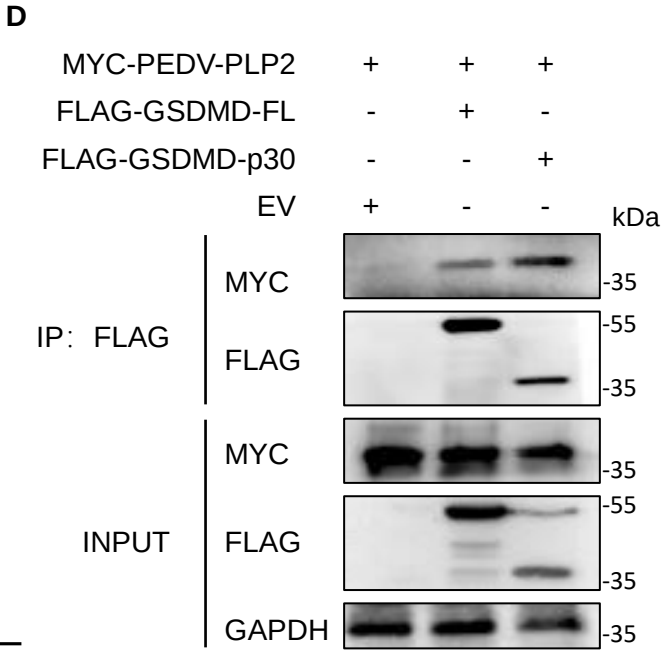
D
MYC-PEDV-PLP2 + + +
FLAG-GSDMD-FL - + -
FLAG-GSDMD-p30 - - +
EV + - -
kDa
IP: FLAG
MYC
-35
FLAG
-55
-35
INPUT
MYC
-35
FLAG
-55
-35
GAPDH
-35

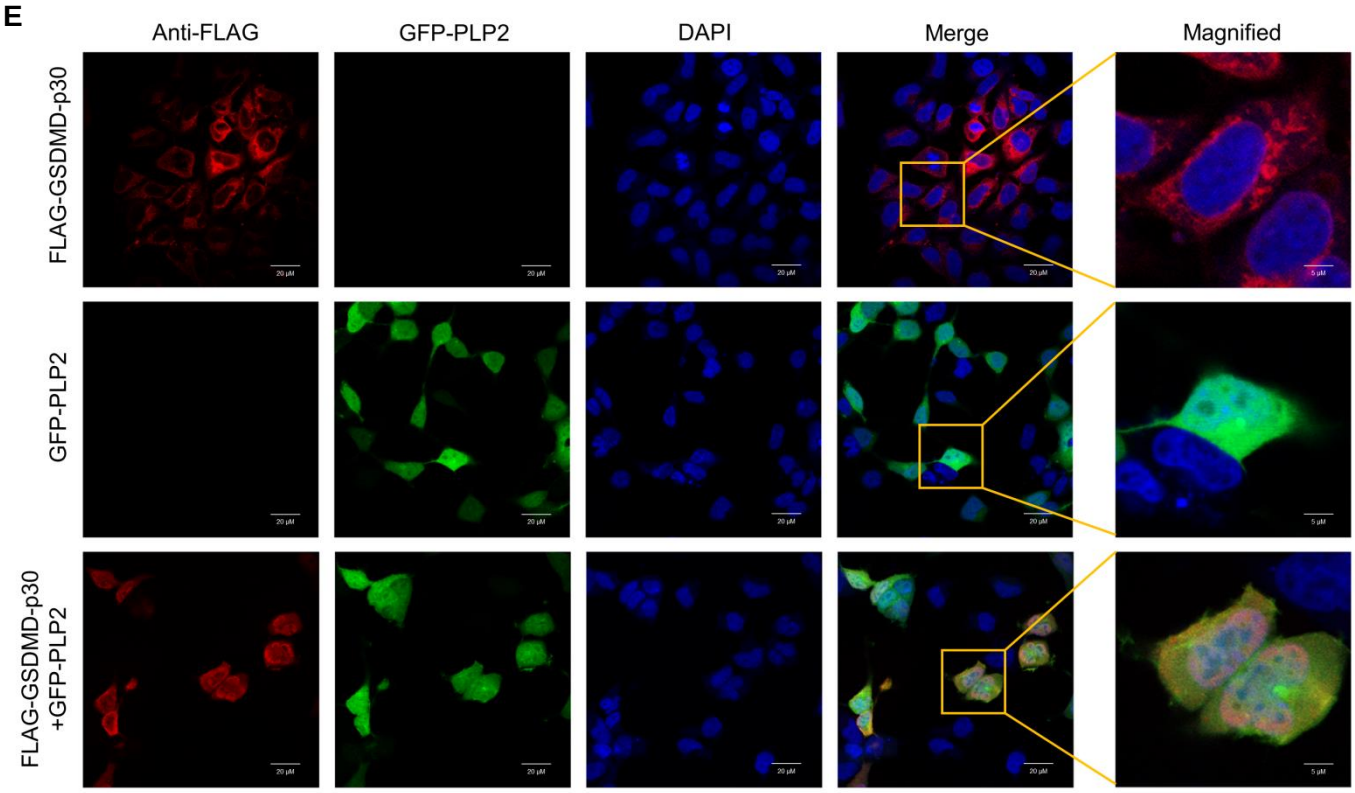
E
Anti-FLAG
GFP-PLP2
DAPI
Merge
Magnified
FLAG-GSDMD-p30
GFP-PLP2
FLAG-GSDMD-p30
+GFP-PLP2

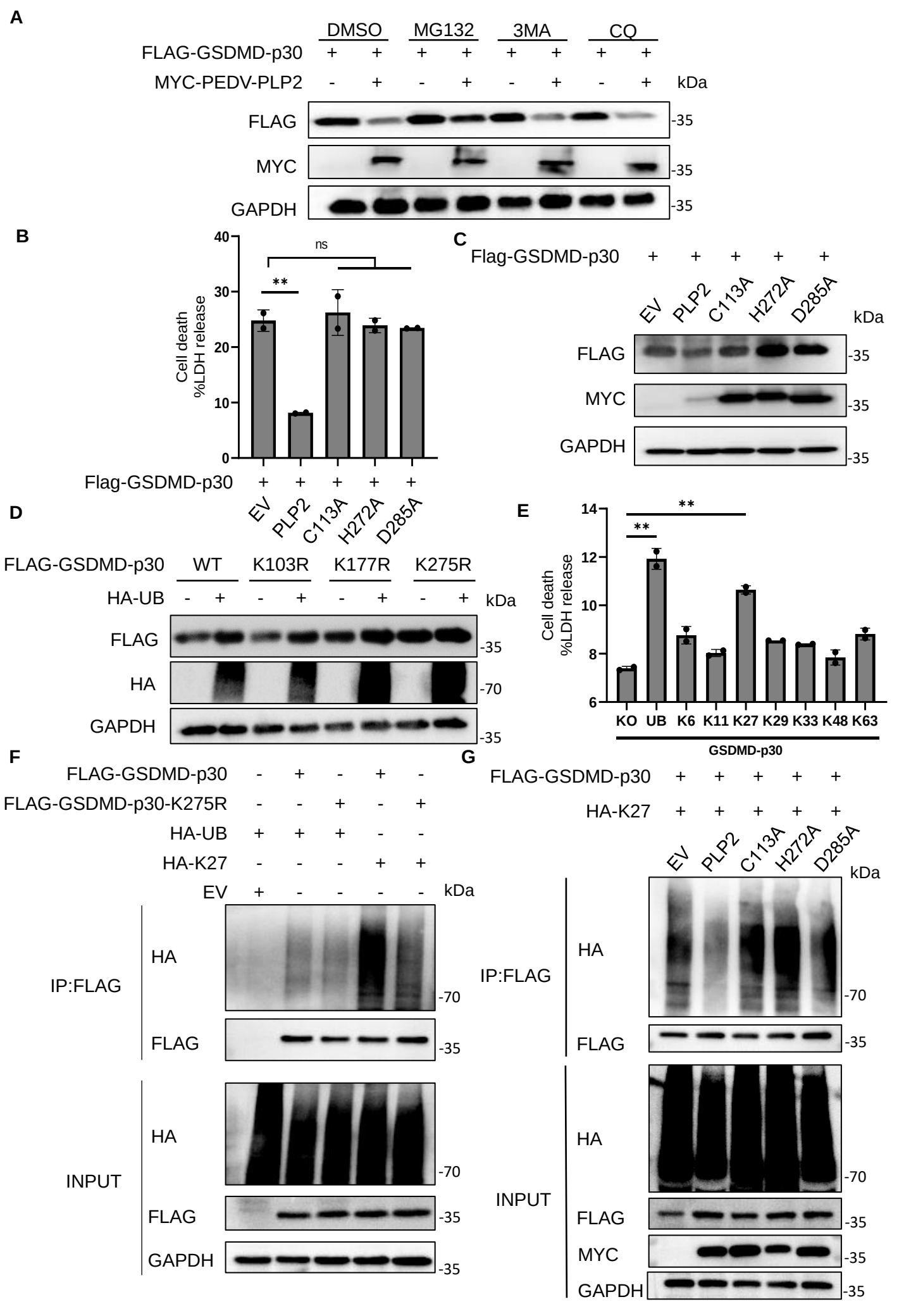
A
DMSO
MG132
3MA
CQ
FLAG-GSDMD-p30
MYC-PEDV-PLP2
kDa
FLAG
MYC
GAPDH
-35
B
Cell death
%LDH release
ns
**
Flag-GSDMD-p30
EV
PLP2
C113A
H272A
D285A
C
Flag-GSDMD-p30
EV
PLP2
C113A
H272A
D285A
kDa
FLAG
MYC
GAPDH
-35
D
FLAG-GSDMD-p30
WT
K103R
K177R
K275R
HA-UB
kDa
FLAG
HA
GAPDH
-35
-70
E
Cell death
%LDH release
**
**
KO
UB
K6
K11
K27
K29
K33
K48
K63
GSDMD-p30
F
FLAG-GSDMD-p30
FLAG-GSDMD-p30-K275R
HA-UB
HA-K27
EV
kDa
IP:FLAG
INPUT
HA
FLAG
GAPDH
-70
-35
G
FLAG-GSDMD-p30
HA-K27
EV
PLP2
C113A
H272A
D285A
kDa
IP:FLAG
INPUT
HA
FLAG
MYC
GAPDH
-70
-35

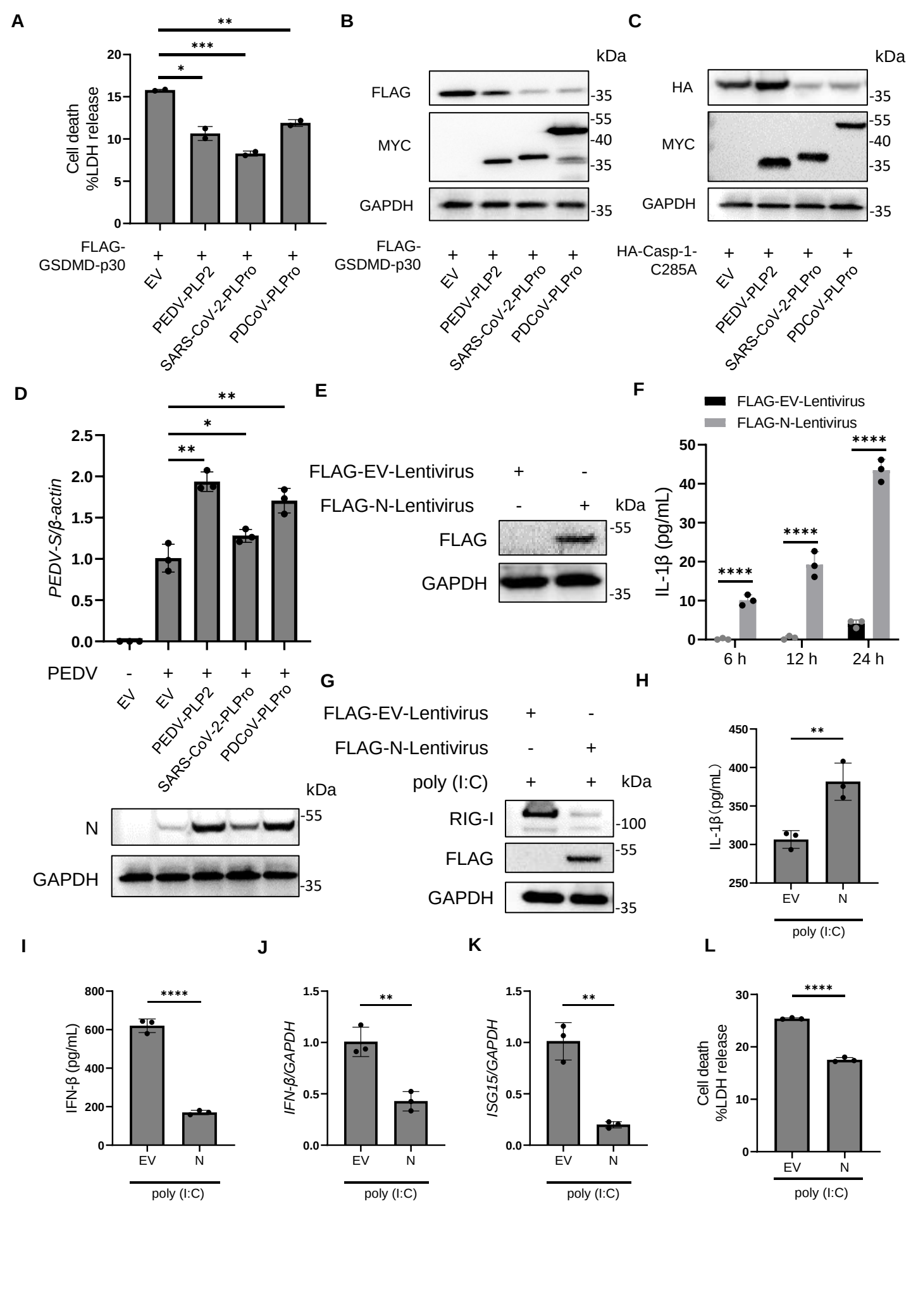
A
Cell death
%LDH release
FLAG-GSDMD-p30
EV
PEDV-PLP2
SARS-CoV-2-PLPro
PDCoV-PLPro
B
kDa
FLAG
MYC
GAPDH
C
HA
HA-Casp-1-C285A
D
PEDV-S/β-actin
PEDV
E
FLAG-EV-Lentivirus
FLAG-N-Lentivirus
F
IL-1β (pg/mL)
6 h
12 h
24 h
G
poly (I:C)
RIG-I
N
H
I
IFN-β (pg/mL)
J
IFN-β/GAPDH
K
ISG15/GAPDH
L

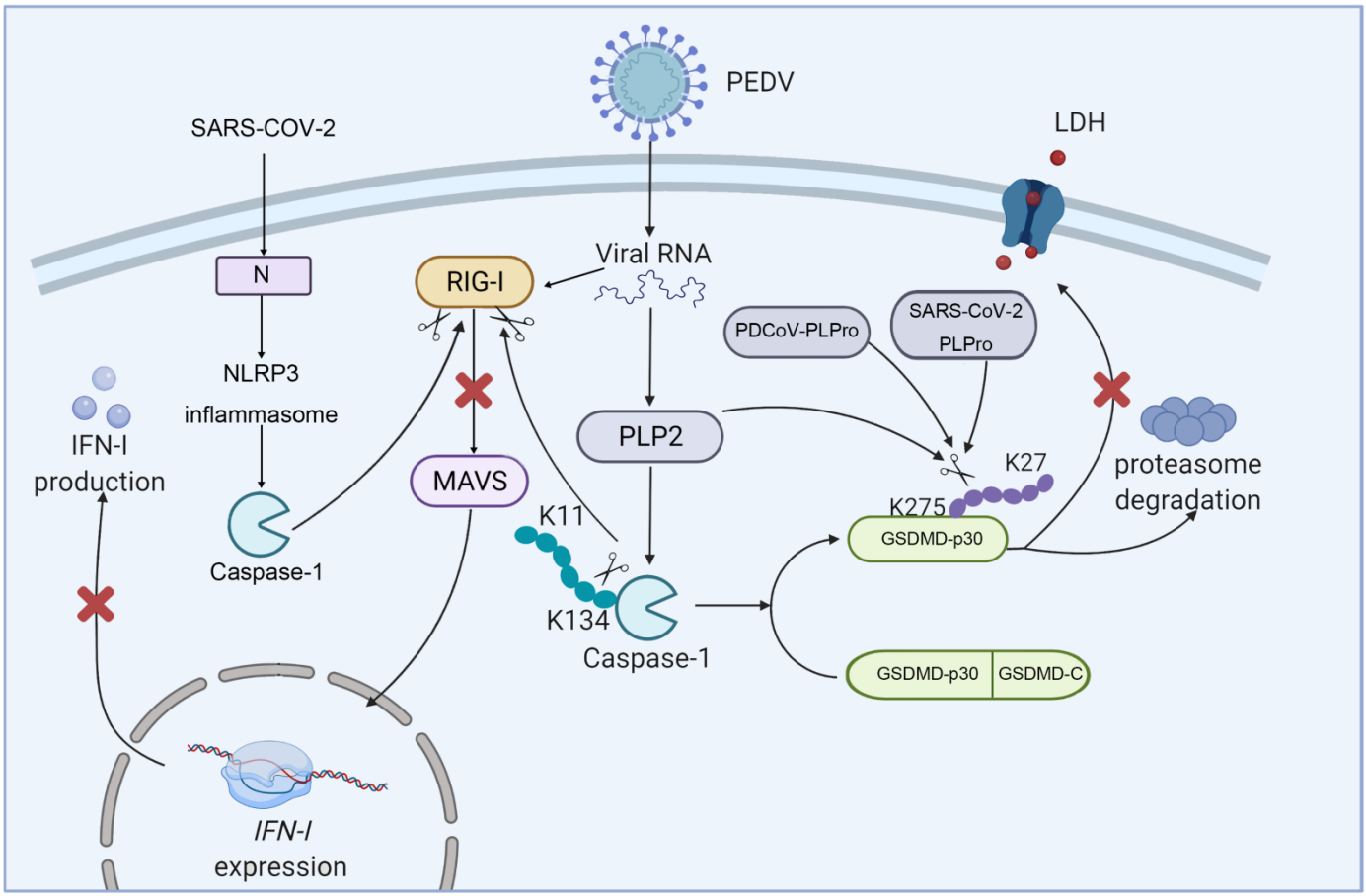
PEDV
SARS-COV-2
LDH
N
RIG-I
Viral RNA
PDCoV-PLPro
SARS-CoV-2
PLPro
NLRP3
inflammasome
IFN-I
production
PLP2
MAVS
K27
proteasome
degradation
K275
K11
GSDMD-p30
Caspase-1
K134
Caspase-1
GSDMD-p30
GSDMD-C
IFN-I
expression